An ontogeny study of cerebral vascular maturation in a sheep model of fetal growth restriction

Degree Project in Medicine

Elisa Lappalainen



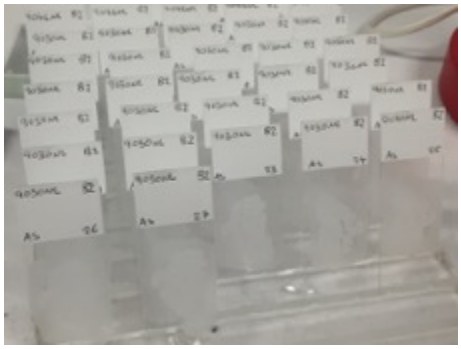
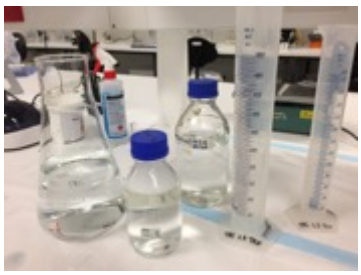
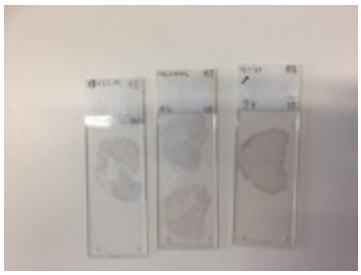
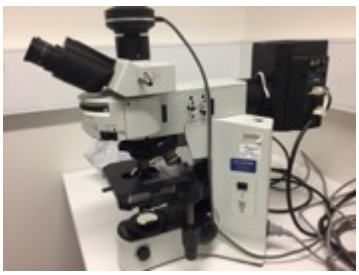
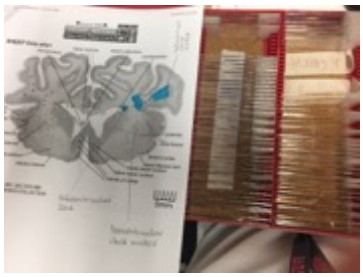

May 28, 2018

University of Gothenburg

THE SAHLGRENSKA ACADEMY

An ontogeny study of cerebral vascular maturation in a sheep model of fetal growth restriction

Degree Project in Medicine

Elisa Lappalainen

Programme in Medicine

2018-05-28

Supervisors: Prof Carina Mallard, A/Prof Suzie Miller, Dr Margie Castillo-Melendez
Department of Physiology, Institute of Neuroscience and Physiology, Gothenburg
The Ritchie Center, Hudson Institute of Medical Research, Clayton, Victoria, Australia

Table of Contents

1. Abbreviations

AGA - appropriate for gestational age

ANOVA = analysis of variance

APIB - assessment of premature infants' behaviour

BBB - blood-brain-barrier

CNS - central nervous system

CP - cerebral palsy

DAB - 3'3 diaminobenzidine

EPC - endothelial progenitor cell

FGR - fetal growth restriction

fig - figure

GA - gestational age

GABA - gamma-aminobutyric acid

GM-IVH- germinal matrix-intraventricular haemorrhage

HRP - horseradish peroxidase

IHC – immunohistochemistry

IUGR - intrauterine growth restriction

IVH - intraventricular hemorrhage

min - minutes

MMP – matrix metalloproteinase

MRI - magnetic resonance imaging

NS - non-significant

NVU - neurovascular unit

PAP – peroxidase-anti-peroxidase

PBS - phosphate-buffered saline

PVWM - periventricular white matter

PWMI - periventricular white matter injury

SCWM - subcortical white matter

SEM - standard error of the mean

SGA- small for gestational age

SUAL - single umbilical artery ligation

SVZ - subventricular zone

UA - umbilical artery

VEGF = vascular endothelial growth factor

2. Abstract

Degree Project

Programme in Medicine

Title: An ontogeny study of cerebral vascular maturation in a sheep model of fetal growth restriction

Author, year: Elisa Lappalainen, 2018

Institution, city, country: Department of Physiology, Institution of Neuroscience and Physiology, Sahlgrenska Academy at University of Gothenburg, Sweden AND The Ritchie Center, Hudson Institute of Medical Research, Clayton, Victoria, Australia

Supervisors: Prof Carina Mallard, A/Prof Suzie Miller, Dr Margie Castillo-Melendez

Background: In fetal growth restriction (FGR), the fetus fails to reach its genetically determined growth potential during gestation. It is most commonly caused by placental insufficiency that leads to chronic hypoxia in utero, affecting neurodevelopment.

Aims: In this experimental ontogeny study, we aim to examine the expression and distribution of laminin, VEGF, MMP9, endoglin and Ki67 in the developing, growth-restricted ovine brains and compare the distribution to appropriately grown, gestational-age matched control animals.

Methods: A growth restricted group and a control group of fetal sheep at 115, 125 and 145 (term) days of gestation were studied in this project. Sections of the periventricular white matter, subcortical white matter and subventricular zone were stained with immunohistochemistry.

Results: The majority of the immunohistochemical markers used in this study showed no statistically significant differences between the FGR group and the control group at the gestational ages and the brain regions examined. Nonetheless, we found significant differences in the blood vessel

morphology parameters and blood vessel density between the gestational ages in several brain regions. We observed vascular expansion at 125 days of gestation. The total number of blood vessels appeared significantly increased in the white matter regions at term gestation compared to the earlier gestational ages regardless of growth restriction. The percentage of MMP9-positive blood vessels differed significantly between the gestational ages in the subcortical white matter of FGR and control animals. In the white matter regions, the results showed a trend of increased vascular proliferation in FGR and control animals at 115 and 125 days of gestation compared to term gestation.

Conclusions: These results suggest a peak in vascular expansion at 125 days of gestation in FGR and control animals. This leads to increased number of blood vessels at term gestation in the white matter regions.

Key words: fetal growth restriction, ontogeny, cerebrovascular development, neurovascular unit

3. Introduction

Fetal growth restriction (FGR), also known as intrauterine growth restriction (IUGR), is a common complication of pregnancy when the fetus fails to gain the endorsed growth potential (1). FGR affects up to 3-9 % of pregnancies in high-income countries (2). A newborn with an estimated fetal weight below the 10th percentile for their sex and gestational age, along with altered placental perfusion during pregnancy, is typically diagnosed with FGR (3). Nevertheless, there is no internationally recognized definition to this phenomenon (2).

3.1. Background

FGR is sometimes defined solely based on birth weight (1). Defining FGR by this way creates confusion between FGR and a condition named small for gestational age (SGA), and these terms are sometimes used synonymously (4). However, because of potentially different aetiologies and postnatal outcomes, these two conditions should be distinguished (1). SGA simply refers to a low birth weight (4). It may be caused by a variety of constitutional and physiological causes, and is not always associated with a pathological outcome (4). This subgroup of small fetuses does not present umbilical cord Doppler signs associated with hemodynamic redistribution, histological or biochemical signs of placental disease or higher risk of preeclampsia (3). “True” FGR refers to small fetuses with a higher risk for fetal in utero deterioration, stillbirth, neonatal death, perinatal morbidity, cerebral palsy (CP), and adult diseases, compared to fetuses appropriate for gestational age (AGA) (3, 4). FGR can be differentiated from SGA by Doppler cerebroplacental ratio (calculated by dividing the middle cerebral artery pulsatility index by the umbilical artery Doppler pulsatility index), by the uterine artery Doppler pulsatility index and by very small estimated fetal weight (among fetuses below the 10th centile, those with an estimated fetal weight < p3) (3).

3.1.1. Causes of fetal growth restriction

The various causes for development of FGR are generally categorized as maternal, fetal and placental (5). Nevertheless, these aspects may overlap each other (5). Fetal causes include fetal infections, chromosomal abnormalities and multiple gestation (1). Maternal factors comprise autoimmune, endocrine and cardiovascular diseases, and drug abuse (1, 2). However, the leading cause of FGR is placental insufficiency (4). Exact mechanisms that result in progressive deterioration in placental function remain unknown (6). In terms of pathophysiology, decreased transfer of oxygen and nutrients via placenta to the fetus leads to fetal hypoxemia and reduced fetal growth (7). In response to hypoxemia, the fetus may react with an abnormal Doppler cerebroplacental ratio, indicative of a brain sparing, a phenomen discussed further in the next section.

The two different phenotypes of FGR in response to placental insufficiency are early-onset, established in the second trimester, and late-onset, established in the third trimester. In early-onset FGR, abnormal placental perfusion is caused by villous damage in the vasculature. This leads to increased umbilical artery (UA) blood flow resistance, increased UA Doppler index and diminished fetal oxygen transfer. In late-onset FGR, villous damage decreases gas and nutrient exchange as well, but the effect on vascular resistance is mild, often followed by normal UA Doppler. (8)

3.1.2. Clinical neurodevelopmental outcome of FGR

What has been observed in growth restricted fetuses is asymmetric fetal growth in which fetal cardiac output is redistributed favoring the brain, called brain sparing (9). Brain sparing leads to elevated brain:body weight ratio (2). However, this compensatory response is insufficient because the brain is not spared in terms of neurodevelopmental outcome (2). The neurological consequences of FGR include increased risk for intraventricular-germinal matrix haemorrhage (GM-IVH) (1), cerebral palsy (CP) (10), poor prenatal head growth (10), behavioral difficulties (11), cognitive

impairment (12), inattention-hyperactivity symptoms (11) and lower school performance (11, 12), compared to appropriately grown children. In addition to the neurological outcomes, FGR is linked to an overall increased risk for perinatal mortality and morbidity, respiratory difficulties, polycythemia, hypoglycaemia and hypothermia (1).

The clinical outcome following FGR is confounded by its timing and often co-existing prematurity (2). When FGR is combined with preterm birth, the risk of cerebral palsy is increased, compared to FGR infants delivered at full-term (13). Arduini et al (14) reported that early-onset FGR fetuses showed delay in behavioural state transitions, i.e time intervals between two different behavioural states, compared to AGA fetuses (14). Harvey et al (15) observed that in early-onset FGR, decreased head growth was linked to lower scores for the general cognitive index, perceptual performance and motor scales (15). Regarding early-onset FGR infants born preterm, fetal cardiovascular compromise correlates to deficits in neurodevelopmental outcome (16). In late-onset FGR, reduction in head growth is related to decreased perceptional performance, motor ability, cognition, concentration ability and short-term memory, followed by poorer school performance (17).

3.1.3. Neuropathology in humans with FGR

Several outcome studies have focused on the alterations in brain development in FGR fetuses and FGR children. Tolsa et al (18) showed that FGR infants born preterm had a reduction in cerebral cortical grey matter volume, intracranial volume and total brain tissue volume on magnetic resonance imaging (MRI), compared to gestational-age matched, AGA infants. These findings correlated with FGR infants showing less mature scores in attention-interaction subdomain of the Assessment of Premature Infants' Behaviour (APIB), measured at term-equivalent age (18). Samuelsen et al (19) observed that the cortical growth was diminished and the cell number in the future brain cortex was reduced in FGR affected fetuses autopsied at 19-41 weeks' gestational age (19). Furthermore, Dubois

et al (20) reported that premature FGR newborns had more profound reduction of cortical surface in relation to sulcation index (the proportion of ventral, lateral and vertex cortical sulci areas according to the brain size) compared to premature, AGA newborns (20).

When it comes to the hippocampus, it has crucial functions for the formation of memory and learning (21). It is shown to be vulnerable when exposed to the hypoxia and undernutrition associated with FGR because of its sensitivity to metabolic disturbances (22). Lodygensky et al (23) noted that FGR infants born preterm showed reduction of grey matter volume in the hippocampus, compared to gestational-age matched AGA infants. This structural difference was followed by FGR infants demonstrating less mature scores in all subdomains of the APIB at term-equivalent age (23).

Advances in brain imaging have greatly progressed the assessment of the FGR brain in infants and children. In terms of brain connectivity, Eixarch et al (24) described that 1-year-old children exposed to FGR had altered connectivity in motor and cortico-striatal-thalamic network on MRI examinations, compared to AGA controls. These results correlated specifically with motor scale and cognitive and socioemotional scale results, respectively (24). Fischi-Gomez et al (25) showed that 6-year-old children born moderately premature with additional FGR showed weaker fractional anisotropy-weighted structural connectivity of cortico-basal ganglia-thalamo-cortical loop connections, compared to AGA controls born moderately premature. These findings were associated with poorer socio-cognitive performance in FGR children (25).

The risk of cerebral white matter injuries is increased in FGR (26, 27). Infants with periventricular white matter injury (PWMI) have immature, poorly perfused cerebral blood vessels (28), implying that vascular supply correlates with white matter injury. Late preterm (34-37 weeks) FGR infants have been shown to have increased incidence of GM-IVH, compared to AGA preterm infants (29). Perinatal brain is most susceptible to hypoxic-ischemic periventricular white matter injury (PWMI), leading to cerebral palsy, at 23-32 weeks of gestation (30). Late oligodendrocyte progenitor cells are

potential targets for ischemic brain injury, since myelination is disrupted in PWMI (30). For these reasons, this study focused on cerebrovascular development in the subcortical and periventricular white matter and the subventricular zone (germinal matrix) in FGR and control individuals in late gestation. FGR was induced at the gestational age that preceded myelination and coincided with vulnerability for white matter injury. The experimental design is described in detail in section 4.1.

3.1.4. Neuropathology in animal models

There are several animal models that have been established, which demonstrate how FGR affects brain structure and development. Basilious et al (31) reviewed the physiological and neurological outcomes of FGR induced by uterine artery ligation in animal models. In rats, mice and guinea pigs, FGR leads to an overall reduction in body weight. Nonetheless, the reduced body weight is not associated with proportional reduction in brain weight in either rats or guinea pigs. Thus, these studies suggest relative brain sparing, similar to that observed in humans with brain sparing (31).

With regard to neuron density, FGR leads to neuronal cell loss and loss of the stratified structure in the cerebral parietal cortex in rats, suggesting abnormal neuronal migration (32). Degenerating axons and neuronal cell bodies are present in the hippocampus, external capsule, entorhinal cortices, cingulate cortex white matter and corpus callosum in a rat model (33). Hypoxia-ischemia induced astrogliosis can be detected in the cerebral white matter in FGR guinea pigs (34) and in the hippocampus, entorhinal and cingulate cortices in FGR rats (33). Inflammatory microgliosis appears in cerebral and cerebellar white matter in FGR guinea pigs (34) and in the cingulate white matter in rats (35).

Myelination plays an essential role in neural maturation and function. FGR guinea pig fetuses have reduced number of myelinating oligodendrocytes in the cerebral cortex and cerebellum, but this deficit does not persist in young adulthood (34). FGR rat pups show a decreased number of pre-

oligodendrocytes and a subsequent delay in myelination (35). In terms of white matter, FGR leads to white matter hypomyelination and axonal damage in the brains of fetal sheep (36). Tolcos et al (34) used a guinea pig model and demonstrated reduced cerebral and cerebellar white matter volume in FGR fetuses and 1-week-old neonates. Nonetheless, control levels in the overall cerebral white matter volume were reached by 8 weeks of age, with a persisting decreased width of corpus callosum in young adult age (34). Even though FGR is related to motor impairment in humans, Delcour et al (37) saw no white matter damage in in the primary motor cortex of FGR rats. Instead, FGR group had a diminished total neuron and GABAergic interneuron density in the somatosensory cortex. Markers indicating apoptosis were increased in several white matter areas (37).

Appropriate neuronal connectivity is crucial for higher-order cognitive and motor behaviours (38). Eixarch et al (39) noted that FGR rabbit pups showed a different brain diffusivity pattern in magnetic resonance imaging (MRI) in the grey and white matter of multiple brain regions, compared to appropriately grown controls. MRI diffusion findings correlated with observed neurobehavioral impairments (39). Regarding the structure of the hippocampus, decreased hippocampal volume at birth appeared in a FGR rat model (40). Neuronal density was decreased in the hippocampus of a guinea pig model (41). Illa et al (42) demonstrated that FGR rabbits at 70+ postnatal days presented a higher degree of anxiety, attention and memory problems than control animals. These are some of the cognitive and neuropsychological features described in FGR children (42).

Regarding the gestational age in which FGR is induced, Rocha et al (43) showed that early-onset FGR differs from late-onset FGR in terms of neuropathological outcome in fetal sheep. Early-onset FGR led to progressive hypoxia during the first 10 days of placental insufficiency and resulted in more severe brain damage compared to late-onset FGR. Neuropathological outcome comprised white matter hypomyelination, loss of cortical organization, loss of neuronal integrity in the grey matter, and neuroinflammation with reactive astrogliosis. Late-onset FGR resulted in an immediate acute fetal hypoxic response after induction of placental insufficiency, followed by chronic hypoxia.

Increased apoptosis within the cortex, in the cortical white matter and subventricular zone were identified in the late-onset FGR animals. In both late-onset and early-onset FGR groups, neuropathological findings included mature oligodendrocyte cell loss and a trend towards increased degeneration of cortical neurons, compared to control animals (43)

3.1.5. The cerebral vasculature and the neurovascular unit

The basic cellular and histological structure forming the interactions between the blood vessels of the brain, and the brain parenchyma, are the neurovascular unit (NVU, figure 1) and the blood-brain-barrier (BBB). The definition of the BBB has varied over the past decades, but the current literature on this subject has been reviewed in detail by Hawkings et al (44) and Obermeier et al (45). The BBB functions as a selective diffusion barrier at the level of the cerebral microvascular endothelium, separating the central nervous system (CNS) brain parenchyma from the peripheral blood circulation. The BBB maintains the optimal brain homeostasis by controlling the passage of molecules and ions, delivering nutrients and oxygen, and by protecting the brain from toxins and pathogens (44, 45).

The BBB comprises a single layer of endothelial cells surrounding the circumference of a cerebral capillary lumen (44). Compared to endothelial cells in the periphery, endothelial cells of the BBB have increased mitochondrial content, lack fenestrations and have minimal pinocytotic activity (44). The opposing membranes of the endothelial cells are connected by continuous intercellular tight junctions which limit the movement of molecules through the endothelial cell layer, essentially into the brain (46). Immune cell infiltration to the healthy CNS is prevented by a low expression of endothelial cell leukocyte adhesion molecules (47).

In order to secure adequately supply of oxygen and nutrients to the brain parenchyma, cerebral blood vessels need to build up an appropriate network (48). The neurovascular unit is composed of groups of neurons and their associated astrocytes, interacting with smooth muscle cells and endothelial cells

on the microvessels, pericytes, microglial cells, and the basement membrane that encloses the endothelial cells (44-46). Cells within the NVU work as a complex network (45). They provide functional and structural support to the BBB, maintain brain homeostasis and the integrity of the BBB (48). As a whole, the NVU regulates cerebral blood flow and provides growth factors that contribute to appropriate oxygen and nutrient supply necessary for normal brain development (45, 48).

When it comes to pericytes and astrocytes, pericytes share a common basement membrane with endothelial cells and regulate BBB permeability, cerebral blood flow and clearance of toxic cellular by-products (49). CNS vascular endothelium has increased pericyte coverage compared to peripheral tissues (49). Astrocytes perform neurovascular tasks including providing nutrition for neurons, buffering extracellular potassium balance, regulating neurotransmitter release, controlling immune reaction and forming the BBB (50).

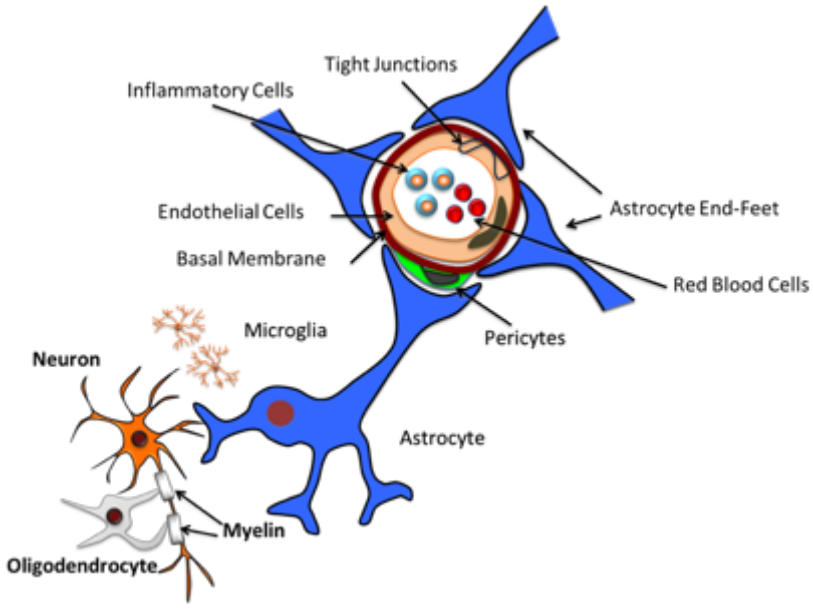

Figure 1 The components of the neurovascular unit. The image used with permission of Dr Margie Castillo-Melendez. "Basal membrane" is used synonymously with "basement membrane".

With regard to the structure of the basement membrane, it comprises collagen type IV, elastin, fibrillin, laminin, fibronectin, cell adhesion molecules, and extracellular matrix and signalling proteins (51). The endothelial cells interact with laminin, collagen type IV and other matrix proteins which anchor the endothelial cells to the basement membrane (52). Matrix proteins boost the expression of endothelial tight junction proteins, making the basement membrane an important player in maintaining the tight junctions (52). Cell-matrix interactions are involved in intracellular signalling pathways (52). In pathological conditions, for example glioblastoma multiforme, changes in the molecular composition of the endothelial tight junctions and the basement membrane can be observed (53). Schöller et al (54) found that the microvascular basement membrane damage correlates with BBB disruption. This suggests that the basement membrane restricts extravasation of proteins into the brain parenchyma (54).

3.1.6. Cerebrovascular development at the molecular level

Brain vascularisation during embryogenetic, fetal and newborn period is a complex process that involves a large number of cells and growth factors (55). It begins with vasculogenesis in which endothelial progenitor cells (EPC) differentiate into endothelial cells forming a primitive capillary network (55). Vasculogenesis is followed by angiogenesis which refers to formation of blood vessels by proliferation, migration and remodelling of endothelial cells into avascular tissue and sprouting of capillaries from pre-existing vessel networks (55).

In angiogenesis, matrix metalloproteinases (MMPs) are a family of proteins that control degradation of the extracellular matrix of the basement membrane (56). Endothelial cell migration and proliferation is then accomplished by activation of chemoattractants and mitogens (56). Next, tube formation takes place, followed by reconstitution of a basement membrane (56). Korzhevskii et al (57) showed that in the developing human telencephalon, the first intracerebral blood vessels are

formed from 7 weeks of gestation. They observed that primitive capillary network appears first, followed by formation of the basement membrane (57).

Endoglin is a transmembrane glycoprotein that can be used as an endothelial cell marker (58). It is expressed in proliferating endothelial cells in the blood vessel endothelium, and its expression is increased during angiogenesis (58). Moving on to consider laminin, it is a non-collagenous glycoprotein that consists of two polypeptide chains joined by disulphide bonds (59). Its expression indicates early vascular development (60). Together with collagen type IV, laminin supports the structure of the basement membrane (61). Deposition of laminin facilitates maturation of capillaries and inhibits cell migration and proliferation (56). In the more mature and adult brain, laminin is only expressed in the basement membrane (62). However, during brain development, laminin is expressed by precursors of neurons and glial cells, suggesting laminin may play a role in neuronal migration (62). In response to brain injury, laminin expression is induced in mature astrocytes (63). Milner et al (64) found that maturation of blood vessels was associated with up-regulation of laminin expression in the developing mouse central nervous system (64).

In terms of cell proliferation, Ki67 is a protein that appears during all active phases of the cell cycle (65). During interphase, it is expressed solely within the nucleus, and during mitosis it is located on the surface of the chromosomes (65). It is absent in resting cells and can therefore be used as a proliferation biomarker that labels cell growth in a cell population (65). It is also used as a prognostic biomarker and to predict treatment response in solid tumours (66). In response to injury, Ki67 is expressed in proliferating cells in the vasculature (67).

A significant protein in terms of vascular development is vascular endothelial growth factor (VEGF), a disulphide-linked dimeric glycoprotein that regulates endothelial cell growth and proliferation, angiogenesis and vascular permeability (68). Physiological and pathological angiogenesis is stimulated by VEGF in a dose-dependent manner (69). VEGF promotes axonal outgrowth, Schwann

cell proliferation, and nerve cell and Schwann cell survival in the superior cervical ganglia and dorsal root ganglia in an adult mouse model (70). During physiologic conditions in the brain, VEGF is mainly expressed by choroid plexus epithelial cells, astrocytes and microglia (71). VEGF may be involved in ingrowth of capillaries from the perineural vascular plexus (72).

3.1.7. Angiogenic response to hypoxia-ischemia

Hypoxia-ischemia affects the cerebral vasculature in several ways. Focal cerebral ischemia induces an immediate breakdown of the primary endothelial cell permeability barrier, expression of matrix metalloproteinases, and appearance of receptors associated with angiogenesis and neovascularization (new blood vessel formation) in cerebral microvessels (73). Krupinski et al (74) observed angiogenic activity in human postmortem brain tissue after stroke. The number of microvessels was higher in infarcted brain tissue compared to the contralateral normal hemisphere, and increased number of blood vessels correlated with longer survival. Infarcted hemispheres had lower number of microvessels filled with blood cells, but the number of empty ones was higher (74).

Baburamani et al (75) demonstrated that a 10-minute, severe, acute hypoxic insult induced by umbilical cord occlusion led to decreased vascular density in caudate nucleus in late-gestation fetal sheep. Furthermore, the number of blood vessels ≤ 10μm of perimeter was relatively decreased and the number of blood vessels ≤ 100μm of perimeter was relatively increased in the periventricular and subcortical white matter, compared to control animals not exposed to hypoxia. This enlargement of blood vessels remained in the white matter for up to 48 hours following the brief hypoxic insult (75). Nonetheless, Castillo-Melendez et al (48) found no significant differences in vascular morphology in the white matter of full-gestation fetal sheep exposed to chronic hypoxia in utero (FGR animals) compared to gestational-age matched, appropriately grown control animals. Instead, they showed reduced blood vessel density in the subcortical and periventricular white matter and the

subventricular zone in FGR animals. They reported also that pericyte coverage of the blood vessels and the number of peri-vascular astrocytes in the white matter regions examined were lower in the FGR group (48).

Apart from angiogenesis, neovascularization after focal cerebral ischemia can also occur via de novo formation of blood vessels, vasculogenesis (55). Endothelial progenitor cells (EPC) migrate to the site of the injury, differentiate and release growth factors that contribute to vessel formation (55). Zhang et al (76) showed with an adult mouse model that bone-marrow derived EPC promoted to neovascularization in the brain tissue damaged by ischemia (76).

Regarding the link between hypoxia-ischemia and MMP9, Zalewska et al (77) used a gerbil model and demonstrated that transient cerebral ischemia led to up-regulation of MMP9 in dorsal parts of hippocampus. This was followed by degradation of laminin, substrate of the MMP9, in the CA1 region of the hippocampus. They suggest that the MMP pathway may be involved in delayed neuronal death after short-term global ischemia (77). Reviewed by Rosenberg et al (78), an ischemic insult in the brain activates MMP2, leading to disruption of the BBB. This BBB injury follows a biphasic pattern with a second, more severe disruption 24-48 hours later, associated with brain oedema and haemorrhage. The second phase correlates with increased levels of MMP9. In conclusion, the author suggests that hypoxia-ischemia leads to activation of the MMPs which results in degradation of the basement membrane and increases the risk of haemorrhage (78).

MMP9 knock-out, adult mice subjected to focal cerebral ischemia are shown to have reduced ischemic lesion volumes (79), reduced BBB disruption (80) and decreased ischemic degradation of the MMP9 substrate, myelin basic protein (80), compared to wild-type mice. Svedin et al (81) studied MMP9 knock-out neonatal mice exposed to hypoxia-ischemia and reported that MMP9 deficiency reduced loss of cerebral tissue and white matter components, delayed and reduced opening of the BBB and decreased inflammation, compared to wild-type animals. (81).

VEGF has been widely studied in the context of hypoxia-ischemia. Reviewed by Hermann and Zechariah (71), hypoxia-ischemia in the brain result in VEGF expression in neurons, microvascular smooth muscle cells, pericytes and leucocytes, and the expression is up-regulated in glial cells (71). Local VEGF administration after stroke contributes to reduced ischemic brain damage and neurologic recovery with sensorimotor, coordination, and cognitive improvements (71). Nevertheless, acute systemic VEGF administration after stroke leads to increased brain injury, haemorrhagic transformation, microvascular injury, inflammation, permeability of the BBB and albumin extravasation (71). Schoch et al (82) observed that hypoxia was associated with increased expression of VEGF and increased vascular permeability in mice brains. Furthermore, levels of VEGF correlated with the severity of the hypoxic insult. Hypoxia-induced effect on vascular permeability disappeared by VEGF inhibition, suggesting that vascular leakage following cerebral hypoxia is associated with VEGF (82). On the other hand, distribution of VEGF and the vascular proliferation were decreased in the full-term lamb brain exposed to chronic hypoxia in utero (48).

When it comes to the impact of hypoxia-ischemia on BBB stability, hypoxia with reoxygenation is shown to modify tight junction protein expression in cerebral blood vessels in adult rats, suggesting that this reorganization leads to altered paracellular diffusion in the BBB (83). The first cells that react to brain hypoxia are pericytes, starting to migrate from their original location during the first 2 hours of hypoxia (84). Ferrari et al (85) studied neonatal hypoxia-ischemia using a rat pup model. They observed an increased BBB permeability 1 to 7 days and cerebral oedema 1 to 21 days after the hypoxic-ischemic insult (85). While Ek et al (86) found that hypoxia-ischemia in neonatal mice indicated that the BBB opening occurred early and was normalized by 3 days after insult (86). Castillo-Melendez et al (48) observed albumin extravasation in the white matter of FGR lamb brains, indicating reduced integrity of the BBB. They also noted increased number of microbleeds in the subventricular zone of FGR animals, compared to appropriately grown controls (48).

3.1.8. Summary

In summary, it is well established in adult post mortem human studies and in animal models of hypoxia-ischemia that the BBB and NVU become compromised. This is mediated via an acute upregulation of VEGF, followed by MMP activation and breakdown of the basement membrane. Subsequently, the integrity of the brain is altered, thereby allowing peripheral cells more easy access into the brain. What is not known so far is what happens in the developing brain, and in particular, what happens in response to a chronic hypoxic insult, as occurs with FGR. To examine this, the use of an appropriate and relevant animal model that has been exposed to intrauterine hypoxia, such as to mimic placental insufficiency, is needed. Understanding cerebral vascular changes that take place in relation to the FGR during well identified periods of brain development, during which the fetal brain is particularly susceptible to injury, may allow us to identify potential neuroprotective targets for FGR infants.

3.2. Research question

We hypothesize that placental insufficiency induces a compensatory, angiogenic response in the brains of FGR fetal sheep in early pregnancy. This angiogenetic response is characterized by increased VEGF immunoreactivity, increased MMP9 and Ki67 expression in the cerebral blood vessels and increased total number of cerebral blood vessels in FGR animals, compared to control animals. We want to determine whether this angiogenetic response to reduced placental blood flow is maintained in FGR animals as the hypoxia becomes chronic when the pregnancy approaches full term.

3.2.1. Specific aims:

- In this experimental ontogeny study, we aim to examine distribution of laminin (a major component of the basement membrane), VEGF (one of the most important pro-angiogenic mediators), MMP-9 (degrades the extracellular matrix and promotes angiogenesis), endoglin (expressed on proliferating endothelial cells) and Ki67 (cellular marker for proliferation) in the developing, growth-restricted ovine brains and compare the distribution to appropriately grown, gestational-age matched control animals.
- We aim to compare the distribution of the expression of these proteins in the subcortical and periventricular white matter and the subventricular zone following the induction of placental insufficiency (single umbilical artery ligation) and as the pregnancy progresses to full term using an ovine model of FGR and immunohistochemistry.

4. Material and Methods

The animal work and tissue collection described below was previously performed at Monash Medical Centre except for cutting the tissue. The tissue came from three different studies undertaken 2012, 2014 and 2017 (36, 43, 87). My part in this project was to examine the effect of placental insufficiency on the cerebral vasculature by staining previously collected brain sections with specific immunohistochemistric markers, conducting light microscopy or image viewing software image collection, and analysing the resulting data which is presented on this report.

4.1. Experimental design

We used three cohorts of Border-Leicester cross Merino pregnant ewes. The tissue material came from their fetuses which represented three different gestational ages (GA, in days): 115 GA (early

preterm, corresponds to ~31 weeks in humans), 125 GA (late-preterm, corresponds to ~34 weeks in humans) and full term (fig 2). Each experimental group had its gestational-age matched, appropriately grown control group. Experimental groups and control groups comprised seven animals (n=7). The gestational age at full term delivery ranged 145 ± 0.9 days in the control group and 144 ± 0.6 days in the FGR group, expressed as mean ± SEM (36). The full-term groups are referred to as 145 GA throughout this thesis.

In the 115 and 125 GA groups, we used twin-bearing ewes. One of the twins of the same ewe was growth-restricted and the other one used as a control. In the 145 GA group, we used a growth restricted group and a control group of lambs delivered after singleton, full-term pregnancy. Altogether, there were six animal groups in this project.

4.2. Surgical procedure and animal maintenance

In each of the FGR groups, fetal growth restriction leading to placental insufficiency was surgically induced at 105 GA (fig 2). The surgical procedures have been described in detail in the previous publications that used the same animal cohorts (36, 43, 87). In summary, placental insufficiency was induced by single umbilical artery ligation (SUAL, fig 3) under anaesthesia. Two silk ligatures were placed tightly around one of the umbilical arteries. The fetus was then returned to the uterus. In the groups of 115 GA and 125 GA, the ewes and the fetuses were euthanized at these gestational ages, via a maternal overdose of intravenous pentobarbitone. In the group of 145 GA, the ewes gave birth to their fetuses, and the lambs were euthanized 24 hours postpartum in the same manner as the groups of the two other gestational ages. We chose to induce placental insufficiency specifically at 105 GA because that precedes the myelination process (fig 2) and corresponds to the gestational age with the highest risk for clinical white matter injury in humans (88).

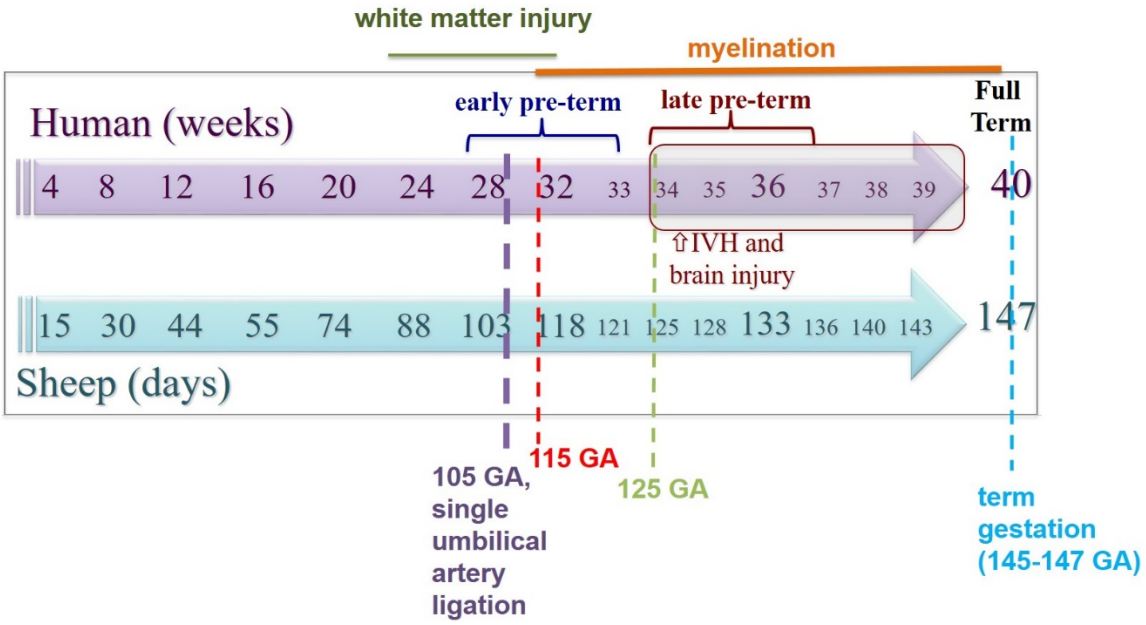

Figure 2 Fetal gestation in humans and sheep. The gestational ages in humans are shown in the purple arrow (weeks), and the corresponding gestational ages in sheep are shown in the blue arrow (days). Late pre-term fetuses have an increased risk of intraventricular hemorrhage (IVH). The human brain is most susceptible for white matter injury at 23-32 weeks of gestation, the developmental window preceding myelination. In this study, placental insufficiency with subsequent fetal growth restriction was induced at 105 days of gestation (105 GA, ~28 weeks of gestation in humans) by single umbilical artery ligation. Growth restricted and control fetuses studied were of three gestational ages: 115 days (115 GA, ~31 weeks in humans), 125 days (125 GA, ~34 weeks in humans) and full-term lambs (145-147 GA). The image adapted with permission of Dr Margie Castillo-Melendez.

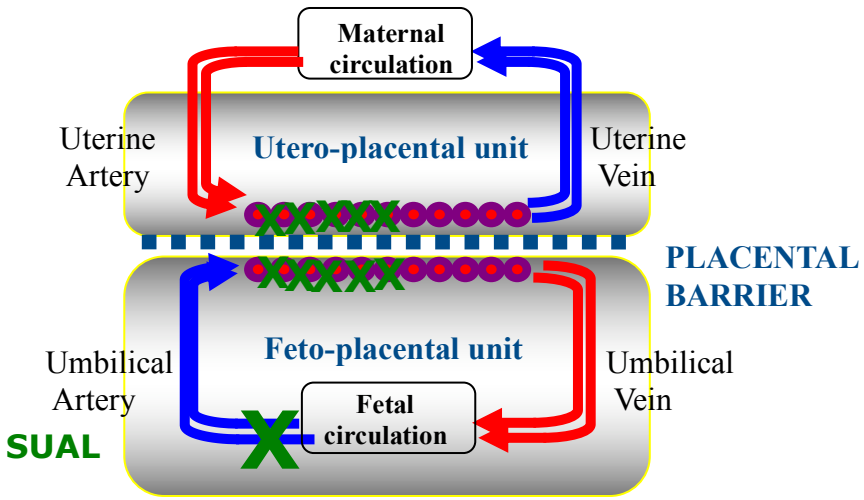

Figure 3 In single umbilical artery ligation (SUAL), one umbilical artery is fully ligated. This causes infarction/death of approximately half of the placental cotyledons, leading to placental insufficiency. This induces progressive fetal hypoxia and hypoglycaemia.

It has previously been shown that placental insufficiency induced by single umbilical artery ligation at 105 GA leads to fetal hypoxemia from day 1 following the surgery, based on fetal arterial blood gas samples (43). In the animals used in this project, the body weights were reduced in FGR individuals compared to controls at all ages (figure 4), but the differences were statistically significant only at 115 and at 145 GA (table 1). However, when the 125 GA animal cohort was previously studied and a higher number of animals was included in the study, there was a statistically significant difference in body weights between FGR and control animals at this gestational age as well (43).

Table 1 Body weights of control lambs and FGR lambs

	Body weight, kg
Control 115 days	1.99±0.127
FGR 115 days	1.59±0.124*
Control 125 days	3.34±0.254
FGR 125 days	2.70±0.149
Control 145 days	4.68±0.227
FGR 145 days	3.37±0.523*

*FGR = fetal growth restriction. Kg = kilograms. Data presented as means ± SEM. *p <0.05: significantly different from control of the corresponding gestational age. Control 115 days = control group at 115 days of gestation. FGR 115 days = growth restricted group at 115 days of gestation. Control 125 days = control group at 125 days of gestation. FGR 125 days = growth restricted group at 125 days of gestation. Control 145 days = control group at term (~ 145 days) gestation. FGR 145 days = growth restricted group at term (~ 145 days) gestation. N= 7.*

Figure 4 A growth restricted lamb at term (left) and an appropriately grown lamb of the corresponding gestational age.

In previous studies with these animal cohorts, it has been shown that there was no significant difference in brain weight between the FGR animals and the control animals in the groups of 125 and 145 GA (36, 43). In the cohorts of 115 and 145 GA, there was a significant increase in brain/body weight ratio in FGR individuals compared to control individuals (36, 87). Decrease in body weight without corresponding decrease in brain weight suggests asymmetric growth restriction and brain sparing. Nevertheless, I was not able to obtain the brain weights for the particular animals I used in my project, so I was unable to determine the brain/body ratios.

4.3. Tissue preparation

The brains were collected, weighed and divided into left and right hemisphere. We used the right hemisphere in my study, which was cut into 0.5 cm coronal blocks and fixed in 10 % buffered formalin or 4 % buffered paraformaldehyde. Three days later, the blocks were fixed in paraffin (fig 5a). During the first weeks of my project, a research assistant cut the blocks into 10 µm coronal sections (fig 5b) at the level of the subventricular zone (SVZ, also known as the germinal matrix). Sections were coded with the animal number and ligated/non-ligated when a twin was used (36, 43).

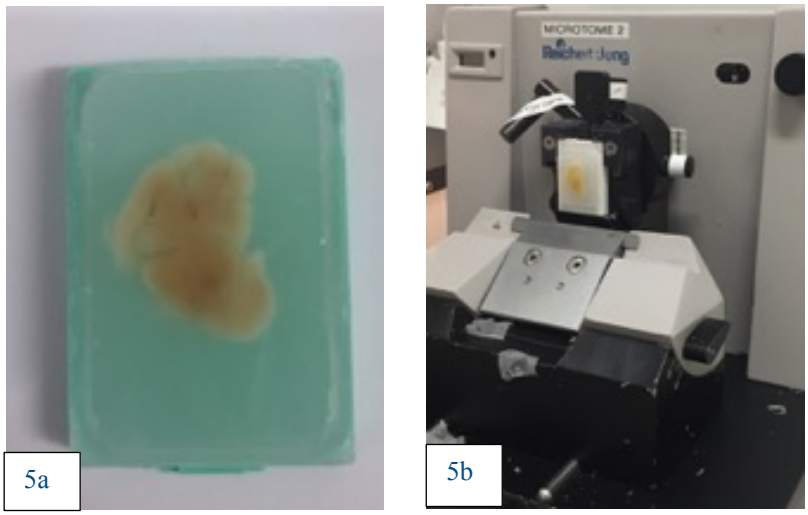

Figure 5a-b. The blocks of brain tissue were embedded in paraffin and cut into 10 µm coronal sections.

We chose to study these particular brain areas and focused on the vascular development because premature infants in combination with FGR suffer from high rates of haemorrhages within the subventricular zone (SVZ) germinal matrix of the brain (89, 90). Furthermore, the risk of white matter injuries is increased in FGR (26, 91).

4.4. Immunohistochemistry

We used immunohistochemistry (IHC) in this study because it allows us to visualize the antigen and identify its localisation and distribution in the tissue (92). A total of five different protocols of indirect IHC were used in this study: single-label IHC for laminin, MMP9, VEGF and Ki67 and a double-label fluorescence IHC for Ki67 and endoglin. Seven animals per group (n=7) and two sections per animal were used for the single-label stainings, making a total of 42 animals and 84 sections. Five animals per group (n=5) were used for the double label fluorescence, making a total of 30 animals and 60 sections.

In every staining, hydrogen peroxide and DAKO protein free blocking solution were used to reduce non-specific background staining. The sections were incubated with a primary antibody the first day, and with a secondary antibody the following day. In the single-label protocols, the staining was visualized with streptavidin-HRP (horseradish peroxidase) and 3,3' diaminobenzidine (DAB) complex. The sections stained for MMP9 and Ki67 were counterstained with cresyl violet. The protocol for single-label, indirect VEGF IHC was performed with practice sections with an intention of later running it on the same animals as I used for the rest of my study. Before completing the protocol for MMP9, optimisation of the protocol was carried out as MMP9 was an IHC marker not previously used by my research group.

All detailed protocols for the five different IHC stainings are found in the appendix of this thesis.

4.5. Tissue Microscopy and Imaging

The stained sections were imaged with a light microscope or a digital image viewing software. The imaging procedures for each staining are described in detail below.

4.5.1. Laminin imaging

The sections stained with laminin were scanned and images were captured at x50 magnification with an image tool Aperio ImageScope [v12.3.2.8013] using a personal computer. Three random fields of view (figure 6) per brain region (subventricular zone, periventricular white matter, subventricular white matter) in each section were taken.

Figure 6. A coronal sections of an ovine brain stained with laminin immunohistochemistry with the target regions imaged in this study. The MMP9 staining and the Ki67 staining were imaged in the same manner. 3 or 4 fields of view per target regions were imaged in each sections. SCWM = subcortical white matter. PVWM = periventricular white matter. SVZ = subventricular zone

4.5.2 MMP9 and Ki67 imaging

Images of the MMP9 and Ki67 staining were taken under a light microscope (Olympus BX41; DP25camera, Olympus, Japan) at x400 magnification. 4 random fields of view per brain region (subventricular zone, periventricular white matter, subventricular white matter) in each section were taken.

5. Data collection procedures

The images for each staining were quantified. The quantification processes are described in detail below. The data from the images was then statistically analyzed, described in detail below.

5.1 Image analysis

The images from the sections stained with laminin were used to assess blood vessel number and morphology. The images stained with MMP9 were used to measure extracellular matrix degradation and promotion of angiogenesis, and the images stained with Ki67 to evaluate endothelial cell proliferation.

5.1.1. Assessment of blood vessel number and morphology (laminin)

All measurements for the sections stained with laminin were carried out with Metamorph Offline (v7.7, Molecular Devices, USA) software. All positive staining that occupied less than 20 pixels was excluded from the analysis. All the data was expressed in pixels and converted to micrometers. The

software gave us the area, perimeter, length and breadth for each individual vessel in every image (figure 7). This was our raw data. From the raw data, the values for all the blood vessels in each image were averaged, and we ended up with an average value for each parameter in each image. The total number of vessels for each image was calculated by the software. The averages were sorted on Excel-sheets by groups, by regions, by animal numbers and by parameters. Images for each animal were averaged so that each animal ended up with one value for vessel area, perimeter, length, breadth and total number of blood vessels per region.

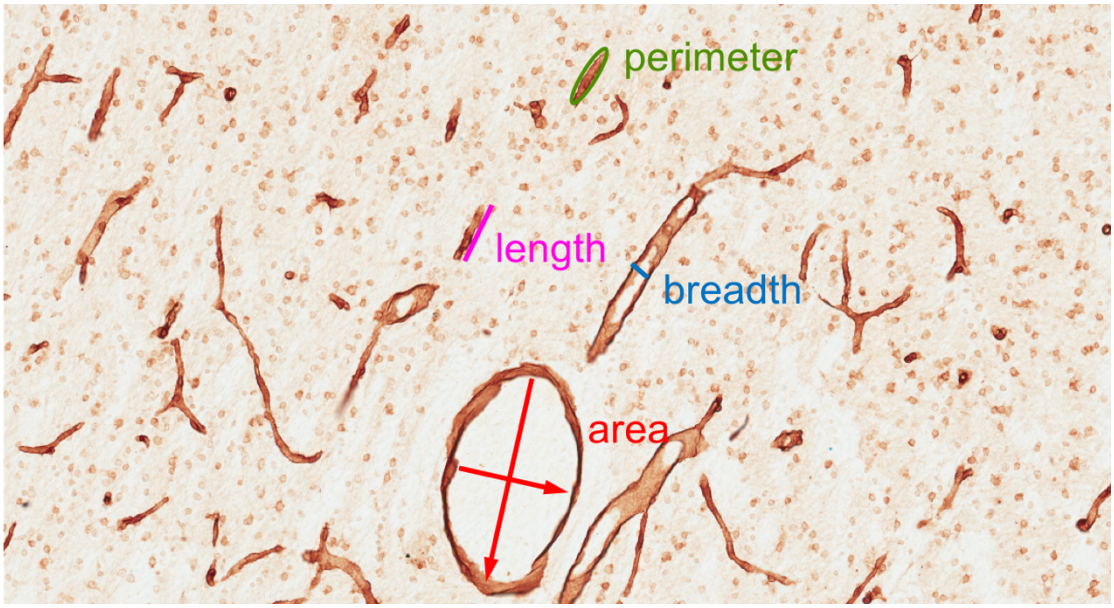

Figure 7 The morphology of the blood vessels was assessed by staining them with laminin immunohistochemistry. The length, perimeter, breadth and area of each blood vessel were calculated with Metamorph Offline software. The values for all the vessels in a field of view were then averaged, resulting in one value per parameter for each field of view. Magnification x100.

5.1.2. Quantification of extracellular matrix degradation and cell proliferation

For the MMP9 and Ki67-staining, the number of MMP9 or Ki67-positive blood vessels were manually counted by Dr Castillo-Melendez blinded to the experimental groups. A total of 4 fields of view per brain region in 2 sections per animal were manually counted using the cell counter plugin on the Fiji software (ImageJ). The total number of blood vessels in a field of view was also counted by her and the number of blood vessels that were MMP9 or Ki67-positive was divided by the total

number of blood vessels in a field of view (figure 8-9). We ended up with the percentage of MMP9 or Ki67-positive blood vessels of all the blood vessels in a field of view. From this raw data, the average percentage was calculated for each animal for each of the brain regions.

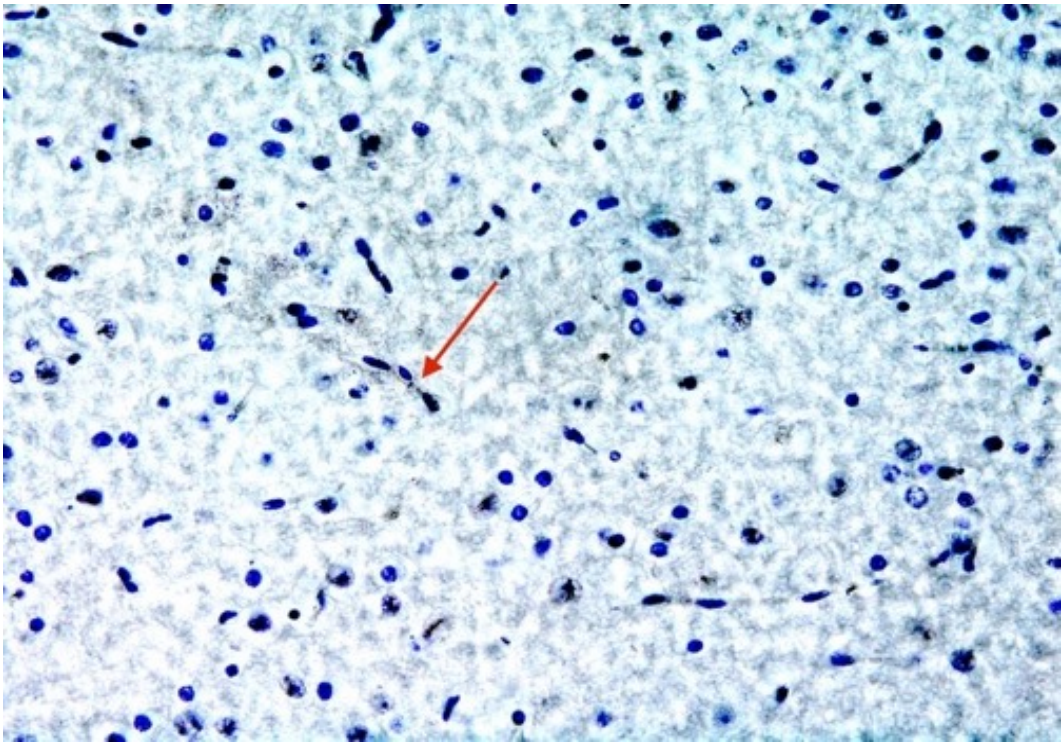

Figure 8 An MMP9-positive blood vessel is marked with a red arrow. The number of MMP9-positive blood vessels was manually counted and divided by the total number of blood vessels in a field of view Magnification x400.

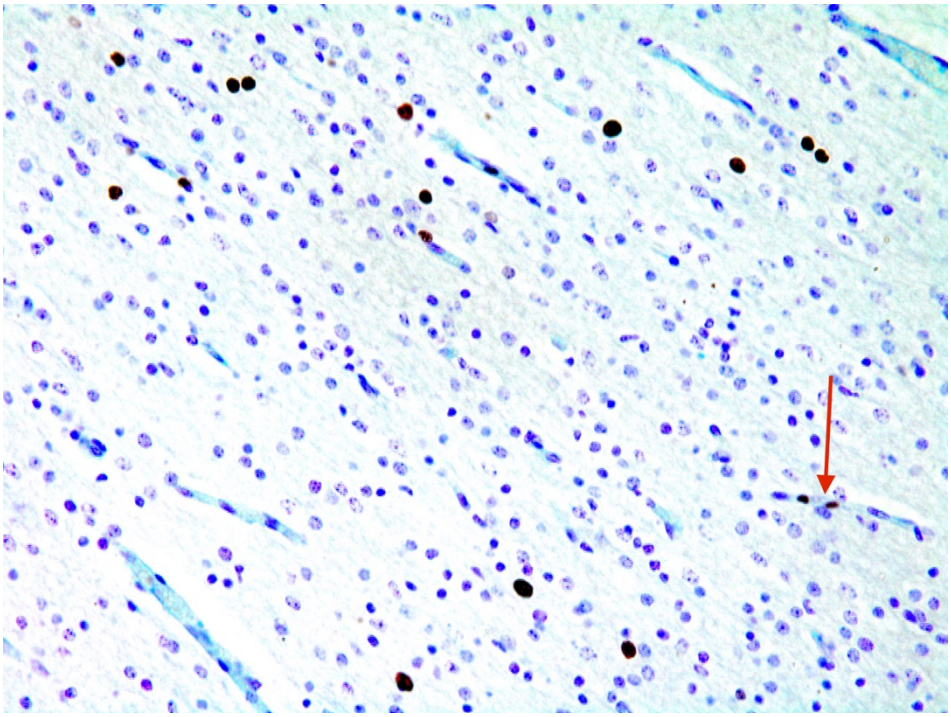

Figure 9 A Ki67-positive blood vessel is marked with a red arrow. The number of Ki67-positive blood vessels was manually counted and divided by the total number of blood vessels in a field of view. Magnification x400.

5.2. Statistical analysis

Visual illustrations and statistical analysis were carried out with Graphpad Prism version 7.0d. Data for each parameter in the brain regions examined was statistically analysed with two-way analysis of variance (ANOVA, comparison between the gestational ages) and post-hoc multiple comparisons test with Bonferroni correction (comparison between FGR and control animals). Prior to running ANOVA, distribution of each data set was analysed with Shapiro-Wilk normality test. The significance was set at $p<0.05$.

6. Ethics

The surgical and experimental procedures undertaken in this project were approved by the Monash Medical Centre Animal Ethics Committee, using guidelines established by the National Health and Medical Research Council of Australia. We wanted to study cerebral vascular adaptations and angiogenetic processes associated with FGR during fetal development. Because of the complexity of this research question and the confounding factors such as prematurity, there is no other way of pursuing this study than using a large animal model with sufficient fetal size and gestational length.

7. Results

The results are presented separately for each staining as images, graphs and statistical results. All data is shown as mean ± standard error of the mean (SEM).

7.1 VEGF immunohistochemistry

This protocol was already established in our laboratory but was performed unsuccessfully due to a change on the antibody clone by the supplier. No staining could be detected using this particular antibody on our test sections, so we chose to not conduct a full run of this particular stain on a larger set of sections.

7.2 Double label fluorescence immunohistochemistry

When the protocol for double label fluorescence for Ki67 and endoglin was completed, and it was time to take pictures with the fluorescence microscope, we found that the staining was too faint due

to decay of fluorescence signal of the Alexa fluorescent secondary antibodies. No good-quality pictures could be taken, thereby we chose to leave this staining out of this project. Nonetheless, we wanted to determine cell proliferation, so we chose to perform a protocol of indirect, single-label Ki67 IHC instead.

7.3 Assessment of blood vessel number and morphology

Representative images of the brain sections stained with laminin immunohistochemistry, sorted by brain regions and by groups, are presented in figure 10. A reduction of laminin staining and decreased blood vessel length and breadth appear in both control and FGR groups at 145 GA compared to 115 and 125 GA groups. However, quantification of the staining was not completely consistent with this observation based on image data. Results from the quantification are explained in detail below (figures 11-15).

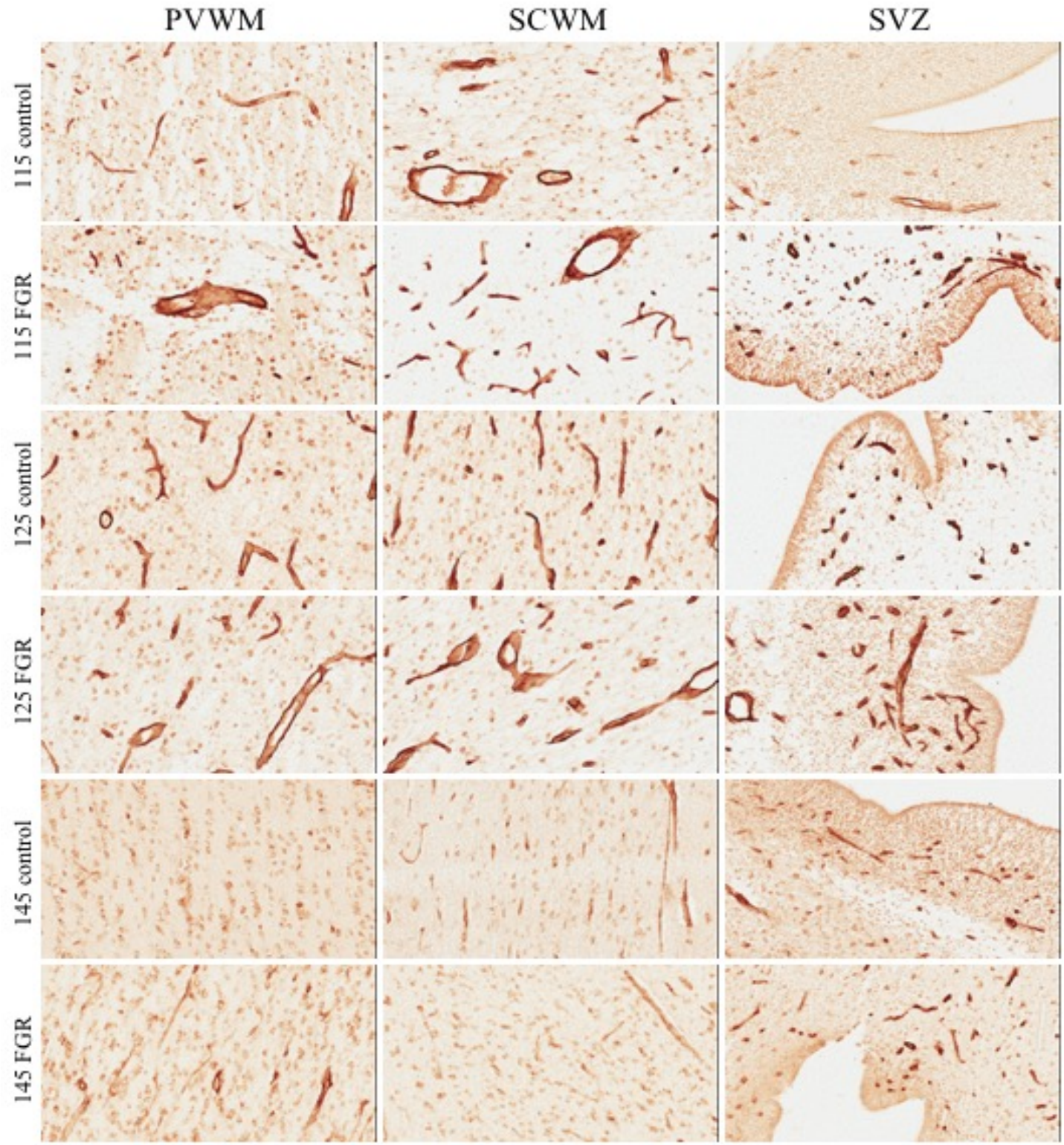

Figure 10. Brain sections stained with laminin immunohistochemistry, x200 magnification. PVWM = periventricular white matter. SCWM = subcortical white matter. SVZ = subventricular zone. 115, 125 and 145 are the gestational ages in days. FGR (fetal growth restriction) represents the groups exposed to placental insufficiency, control represents the appropriately grown control groups.

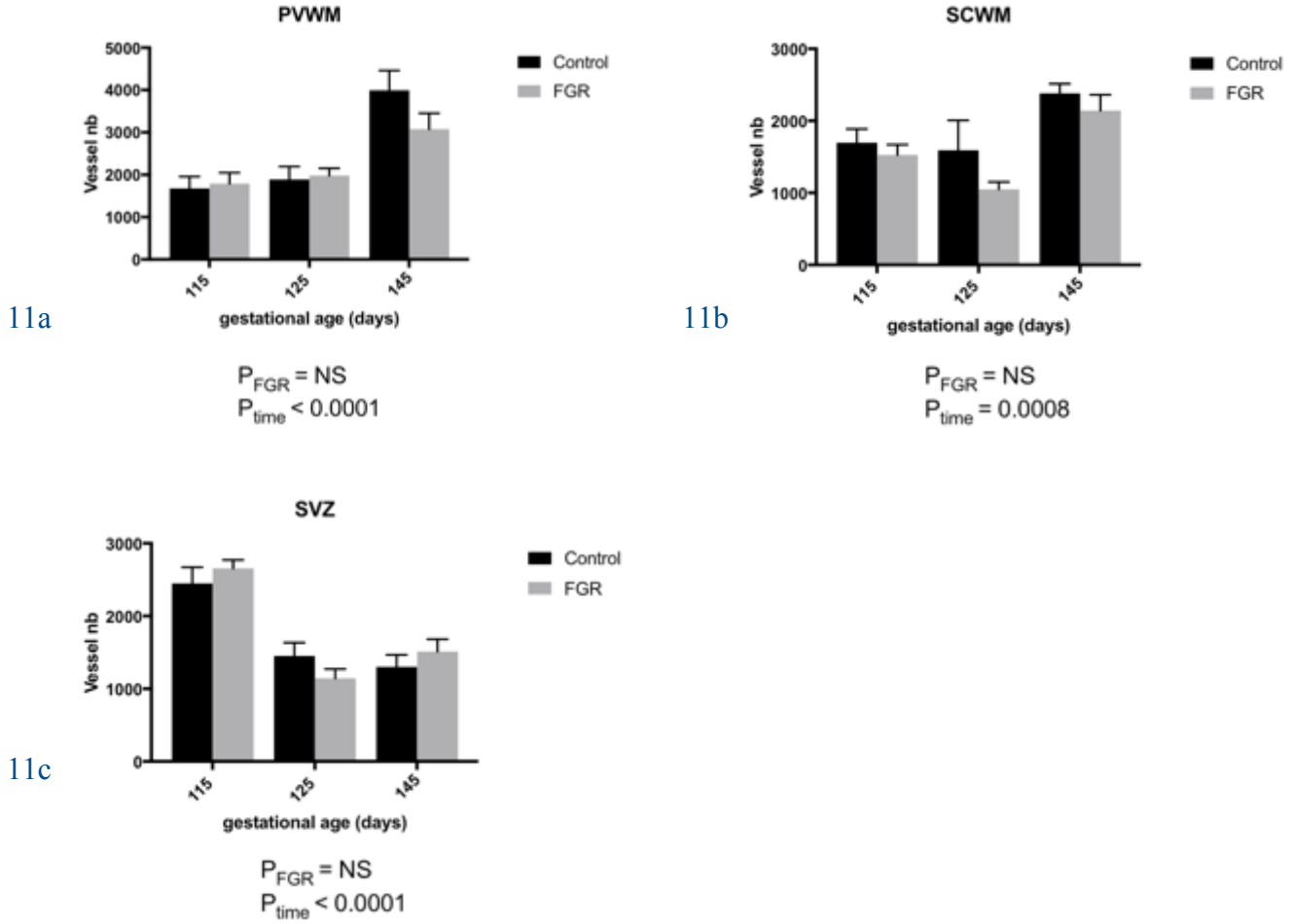

Figure 11a-c. Blood vessel number in a field of view at different gestational ages. P_{FGR} = P-value when the FGR group and the control group of the corresponding gestational ages were compared. P_{time} = P-value when the gestational ages in the same region were compared. NS = non-significant. Data presented as means ± SEM, significance set at P <0.05. Nb=number. PVWM = periventricular white matter. SCWM = subcortical white matter. SVZ = subventricular zone N=6-7 animals/group.

The number of blood vessels in each image was significantly different between the gestational ages in both FGR and control animals in all of the brain regions studied (fig 11a-c). In the white matter regions, there appeared to be an increase in the number of vessels in both the FGR group and the control group at 145 GA, compared to the two earlier gestational ages (fig 11a-b). In the subventricular zone, the number of blood vessels appeared to be decreased at later gestational ages compared to 115 GA in FGR and control animals (fig 11c). No statistically significant differences between the FGR group and the control group were observed in any of the brain regions or gestational ages studied (fig 11a-c).

12a

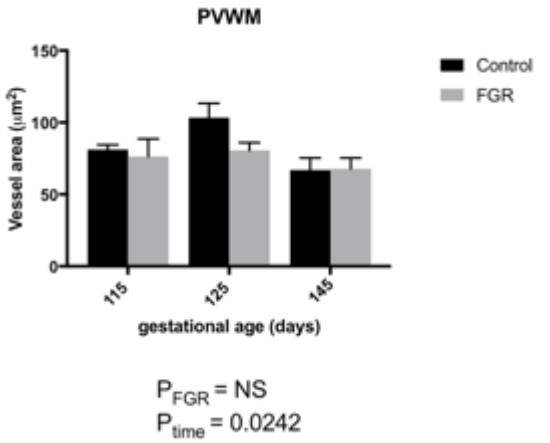

12b

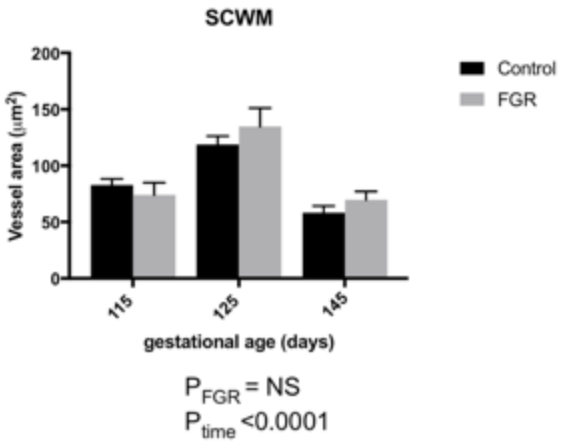

12c

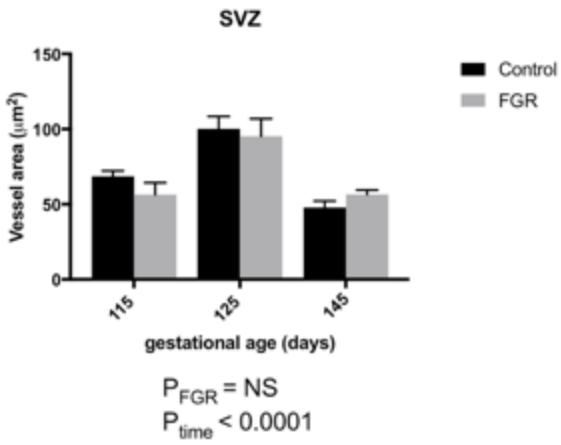

Figure 12a-c. Blood vessel area at different gestational ages in the brain regions studied. P_{FGR} = P-value when the FGR group and the control group of the corresponding gestational ages were compared. P_{time} = P-value when the gestational ages in the same region were compared. NS = non-significant. Data presented as means ± SEM, significance set at P <0.05. PVWM = periventricular white matter. SCWM = subcortical white matter. SVZ = subventricular zone. N =6-7 animals/group.

There were statistically significant differences in the blood vessel area between the gestational ages in all the brain regions studied in FGR and control animals (fig 12a-c). The blood vessel area appeared increased at 125 GA compared to 115 and 145 GA in all the brain regions studied (fig 12a-c). The differences between FGR and control groups did not reach statistical significance in any of the brain regions at any of the gestational ages studied (fig 12a-c).

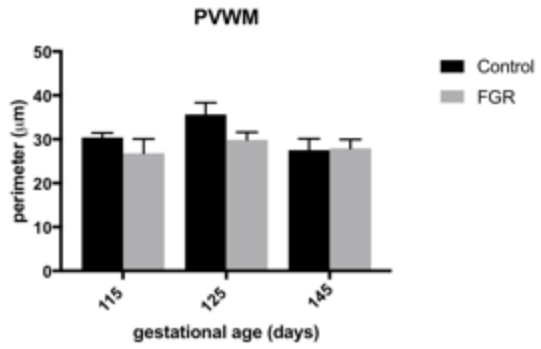

13a

P_{FGR} = NS
P_{time} = NS

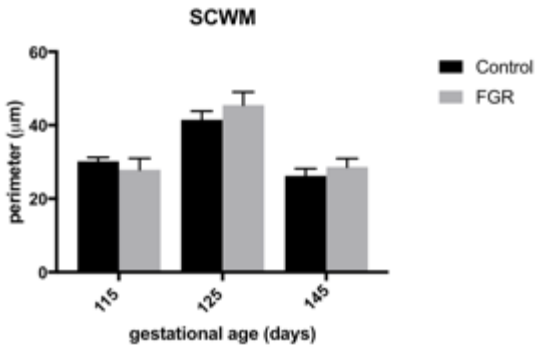

13b

P_{FGR} = NS
P_{time} < 0.0001

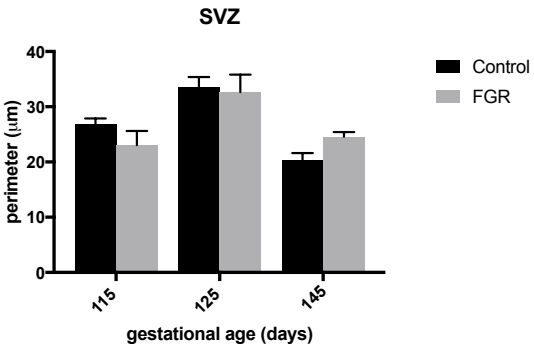

13c

P_{FGR} = NS
P_{time} < 0.0001

Figure 13a-c. Blood vessel perimeter in the brain regions studied. P_{FGR} = P-value when the FGR group and the control group of the corresponding gestational ages were compared. P_{time} = P-value when the gestational ages in the same region were compared. NS = non-significant. Data presented as means ± SEM, significance set at P <0.05. PVWM = periventricular white matter. SCWM = subcortical white matter. SVZ = subventricular zone N=6-7 animals/group.

Blood vessel perimeter was significantly different between the gestational ages in the subcortical white matter and the subventricular zone in FGR and control animals (fig 13b-c). In these regions, the perimeter appeared to be increased at 125 GA, compared to 115 and 145 GA. There were no statistically significant differences in vessel perimeter between the FGR group and the control group in any of the brain regions at any of the gestational ages studied (fig 13a-c).

14a

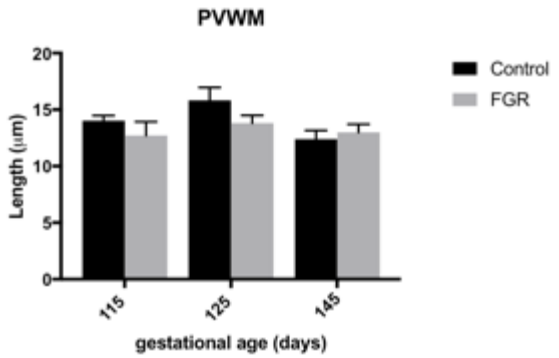

P_{FGR} = NS
P_{time} = NS

14b

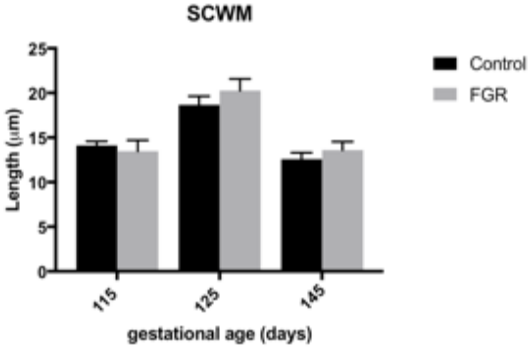

P_{FGR} = NS
P_{time} < 0.0001

14c

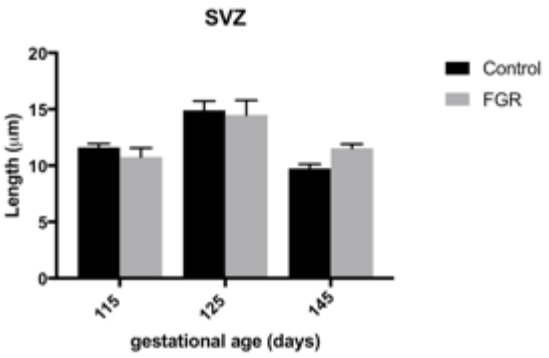

P_{FGR} = NS
P_{time} < 0.0001

Figure 14a-c. Blood vessel length at different gestational ages in the brain regions studied. P_{FGR} = P-value when the FGR group and the control group of the corresponding gestational ages were compared. P_{time} = P-value when the gestational ages in the same region were compared. NS = non-significant. Data presented as means ± SEM, significance set at P <0.05. PVWM = periventricular white matter. SCWM = subcortical white matter. SVZ = subventricular zone N=6-7 animals/group.

Blood vessel length was significantly different between the gestational ages in the subcortical white matter and the subventricular zone in FGR and control animals (fig 14b-c). In these regions, the blood vessel length appeared increased at 125 GA, compared to the two other gestational ages. There were no statistically significant differences between the FGR group and the control group in any of the brain regions at any of the gestational ages studied (figure 14a-c).

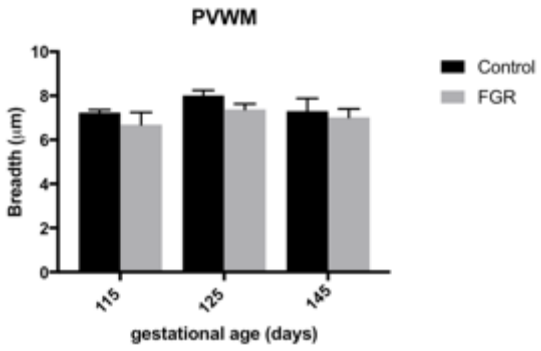

15a

P_{FGR} = NS
P_{time} = NS

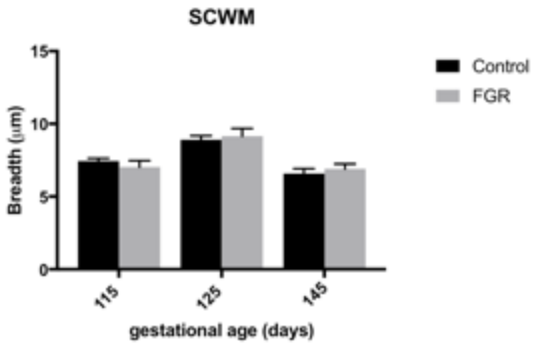

15b

P_{FGR} = NS
P_{time} < 0.0001

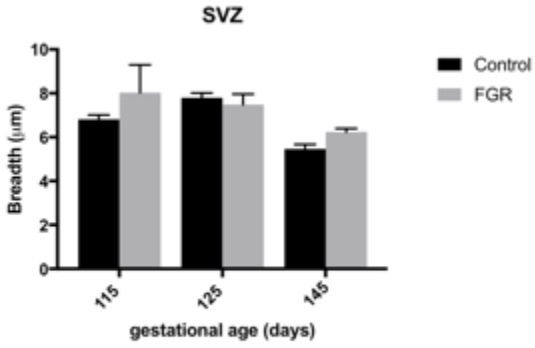

15c

P_{FGR} = NS
P_{time} = 0.0075

Figure 15a-c. Blood vessel breadth at different gestational ages in the brain regions studied. P_{FGR} = P-value when the FGR group and the control group of the corresponding gestational ages were compared. P_{time} = P-value when the gestational ages in the same region were compared. NS = non-significant. Data presented as means ± SEM, significance set at P <0.05. PVWM = periventricular white matter. SCWM = subcortical white matter. SVZ = subventricular zoneN= 6-7 animals/group.

Blood vessel breadth differed significantly between the gestational ages in the subcortical white matter and the subventricular zone in FGR and control animals (fig 15b-c). In the subcortical white matter, vessel breadth appeared increased at 125 GA, compared to the two other gestational ages (fig 15b). In the subventricular zone, vessel breadth appeared decreased at 145 GA, compared to 115 and 125 GA (fig 15c). No differences between the FGR group and the control group reached statistical significance in any of the brain regions at any of the gestational ages studied (15a-c).

7.4 Evaluation of extracellular matrix degradation with MMP9-staining

Representative images of the MMP9-staining are presented in figure 16. MMP9 was mainly located around the blood vessels. Visualization of the blood vessels and MMP9 requires individual adjustments in the light contrast and color exposure using Fiji software and are therefore difficult to see in these images. No clear trends in the distribution of MMP9 could be observed in these images.

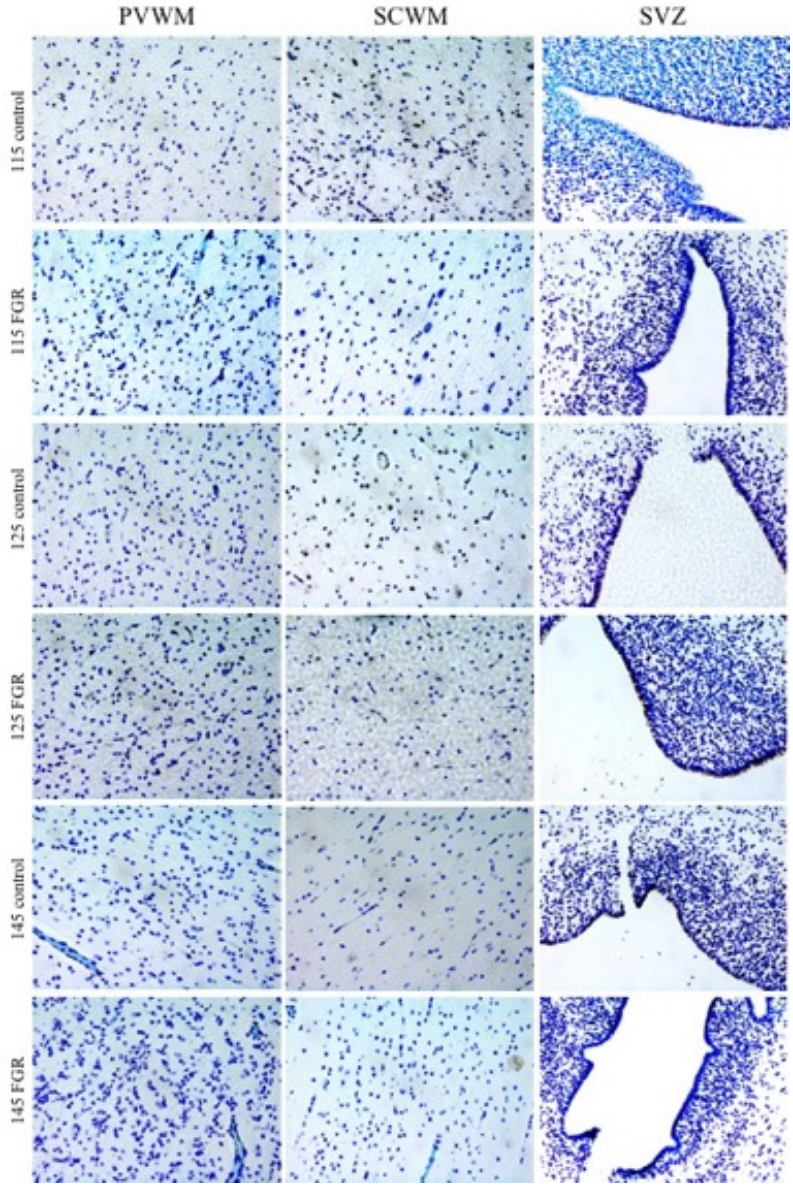

Figure 16. Brain sections stained with matrix metalloproteinase 9 (MMP9) immunohistochemistry, x400 magnification. PVWM = periventricular white matter. SCWM = subcortical white matter. SVZ = subventricular zone. 115, 125 and 145 are the gestational ages in days. FGR (fetal growth restriction) represents the groups exposed to placental insufficiency, control represents the appropriately grown control groups.

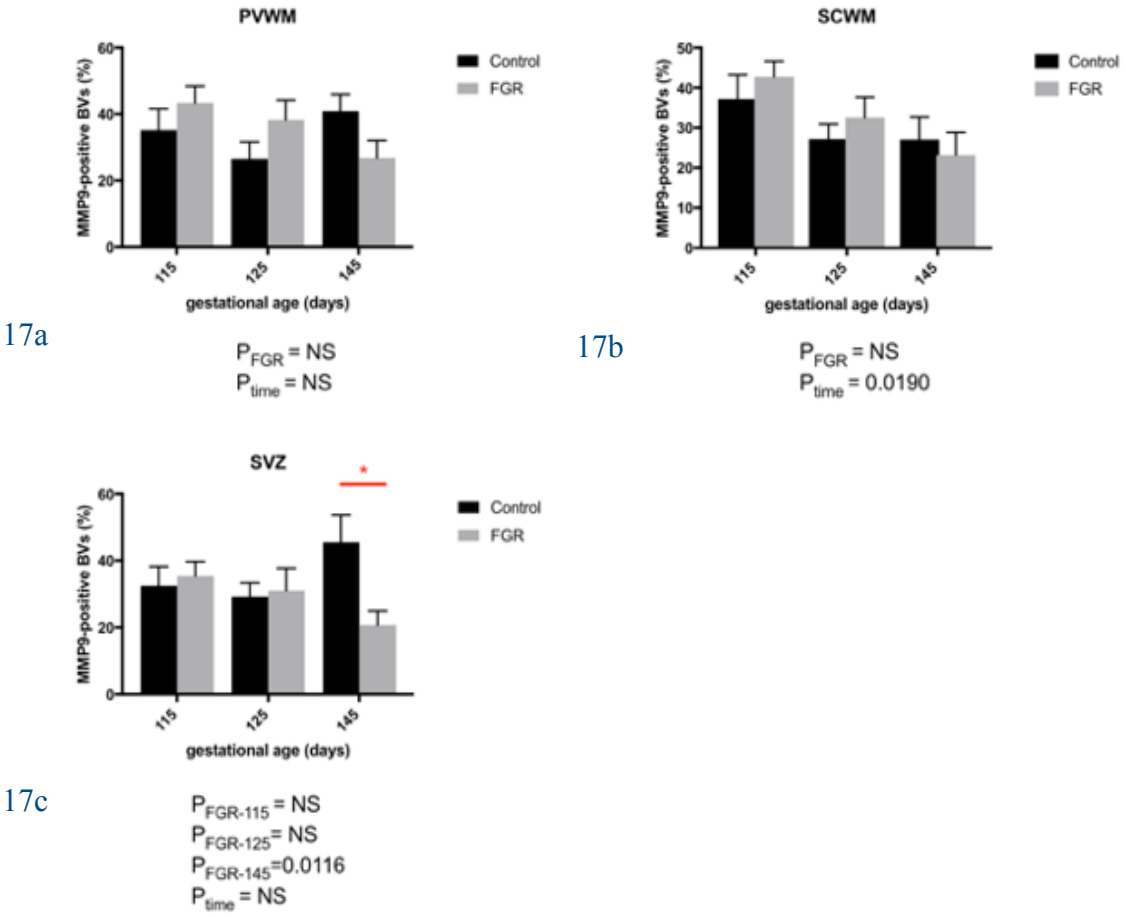

*Figure 17a-c. Percentage of MMP9-positive blood vessels out of the total number of blood vessels in a field of view. P_{FGR} is the P-value when the FGR group was compared to the control group. P_{time} is the P-value when the different gestational ages in the same region were compared. $P_{FGR-115}$, $P_{FGR-125}$ and $P_{FGR,145}$ are the p-values when the FGR group and the control group at 115, 125 and 145 days of gestation, respectively, were compared. NS = non-significant. Data presented as means ± SEM, significance set at P <0.05. * : a statistically significant difference between the FGR group and the control group. BV=blood vessel. PVWM = periventricular white matter. SCWM = subcortical white matter. SVZ = subventricular zone. N=5-7 animals/group.*

In the subcortical white matter, there was a statistically significant difference in the percentage of MMP9-positive blood vessels out of the total number of blood vessels between the gestational ages in FGR and control animals (fig 17b). The percentage MMP9-positive blood vessels appeared to decrease as a function of the gestational age in this region. In the subventricular zone, there was a statistically significant difference between the FGR group and the control group at 145 GA (fig 17c). In the periventricular white matter, there were no statistically significant differences between the gestational ages or between the FGR groups and the control groups (fig 17a)

7.5 Measurement of endothelial cell proliferation with Ki67 staining

Representative images of the Ki67-staining are presented in figure 18. In the 125 GA groups, a trend of higher intensity of Ki67-staining could be observed in the subventricular zone compared to the other regions. Apart from that, no clear trends could be observed based on the image data.

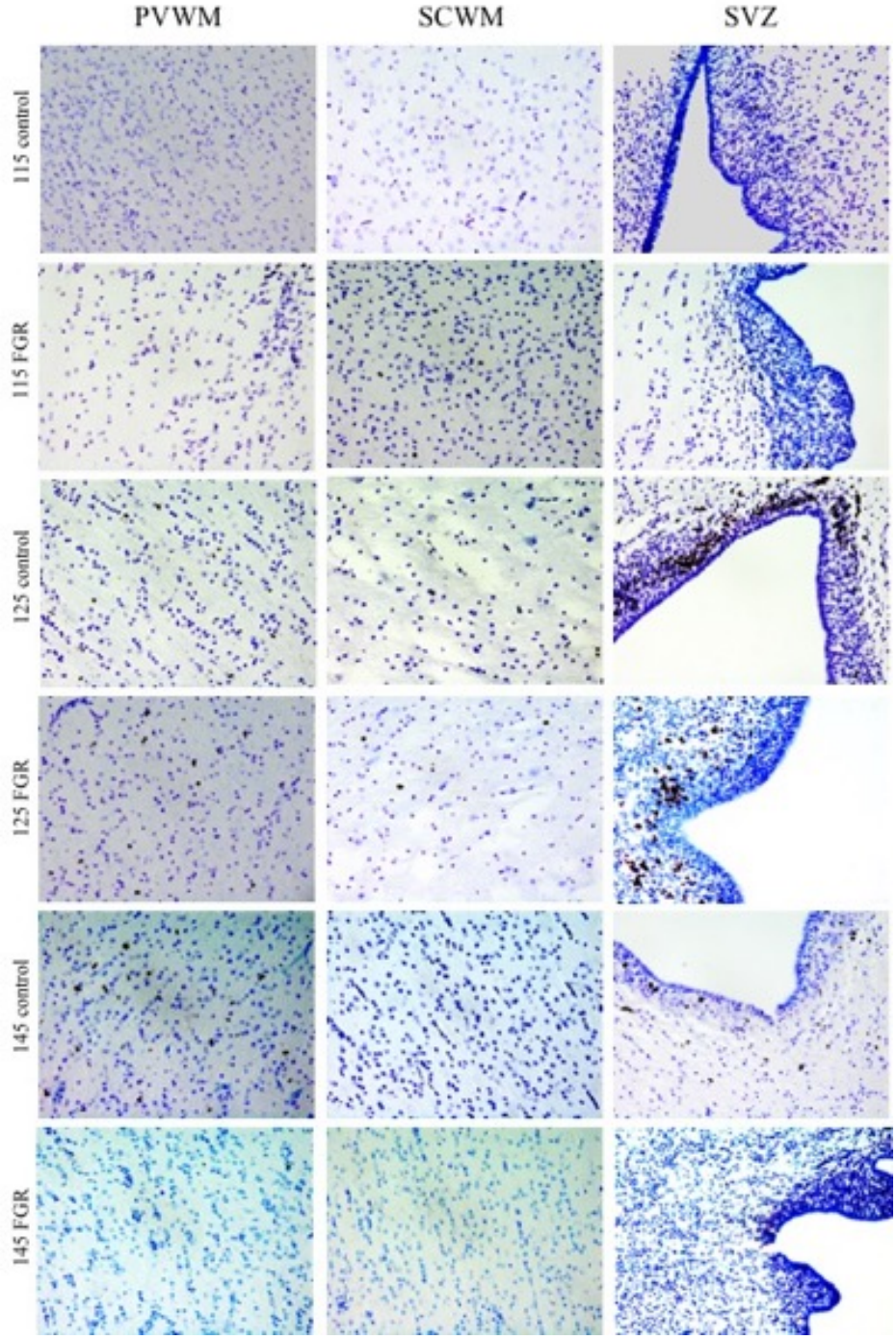

Figure 18. Brain sections stained with Ki67 immunohistochemistry, x400 magnification. PVWM = periventricular white matter. SCWM = subcortical white matter. SVZ = subventricular zone. 115, 125 and 145 are the gestational ages in days. FGR (fetal growth restriction) represents the groups exposed to placental insufficiency, control represents the appropriately grown control groups.

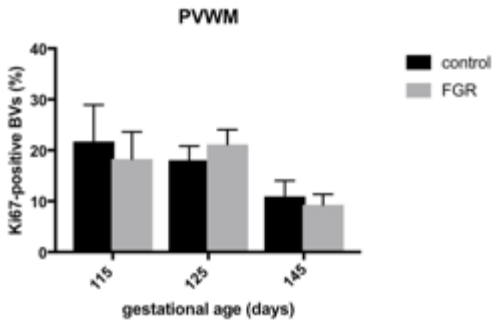

19a

P_{time} = NS
P_{FGR} = NS

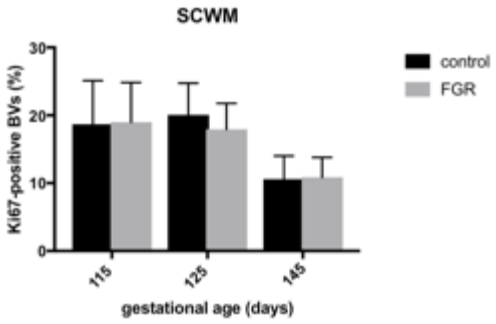

19b

P_{time} = NS
P_{FGR} = NS

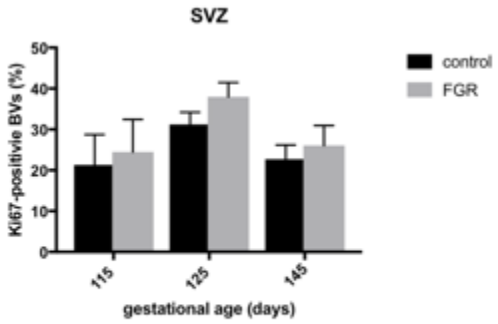

19c

P_{time} = NS
P_{FGR} = NS

Figure 19a-c Percentage of Ki67-positive blood vessels out of the total number of blood vessels in a field of view in different brain regions studied. P_{FGR} = P-value when the FGR group and the control group of the corresponding gestational age were compared. P_{time} = P-value when the gestational ages in the same region were compared. NS = non-significant. BV= blood vessel. Data presented as means ± SEM, significance set at P <0.05. PVWM = periventricular white matter. SCWM= subcortical white matter. SVZ=subventricular zone. N =6-7 animals/group.

There were no statistically significant differences in the percentage of Ki67-positive blood vessels out of the total number of blood vessels between the gestational ages or between the FGR group and the control group in any of the brain regions at any of the gestational ages studied (fig 19a-c). In the subventricular zone, there was a trend of increase in the percentage of Ki67-positive blood vessels at 125 GA in both the FGR group and the control group, compared to 115 GA and 145 GA (p-value 0.1677 between the gestational ages, fig 19c). We could also observe a trend of increase in the percentage of Ki67-positive blood vessels in both FGR group and the control group at 115 and 125 GA compared to 145 GA in the periventricular white matter (p-value 0.0538 between the gestational ages, fig 19a) and in the subcortical white matter (p-value 0.1502 between the gestational ages, fig 19b).

8. Discussion

Germinal matrix and intraventricular hemorrhage (GMH-IVH) are one of the most severe brain injuries in late-preterm babies (93). This ontogeny study evaluated effects of chronic hypoxia on cerebral vasculature during late gestation using a fetal ovine model. We found nearly no differences between the the FGR group and the control group in the parameters we studied. Instead, our key finding is that there were significant differences in the morphology and number of blood vessels between the gestational ages regardless of growth restriction in several brain regions. The area, perimeter, length and breadth of the blood vessels appeared increased at 125 GA, compared to 115 and 145 GA in the corresponding regions. The number of blood vessels appeared increased at 115 GA in the subventricular zone and at 145 GA in the white matter regions, compared to the other gestational ages in the corresponding regions. These differences were most profound in the subcortical white matter and the subventricular zone.

Since the increase in average blood vessel area observed in this study was not accompanied by increased blood vessel number at 125 GA, neovascularization (formation of new blood vessels) is not likely. Our results rather suggest expansion of the existing vessels occurring at 125 GA (~34 weeks GA in humans). Morphological adaptations we observed at this age could be an adaptive vascular response and correlate to previous studies reporting that GMH-IVH rates became significantly elevated in late-preterm births at 34-37 weeks of gestation (29).

Contrary to our results, Mito et al (94) found no major differences in the blood vessel density and morphology in the white matter of the developing human brain (94). Nonetheless, Ballabh et al (89) showed that the vessel density in the human white matter increased only after 32 weeks of gestation and reached its peak at term gestation (89). Authors demonstrated also that the vessel density and percentage of blood vessel area increased from 16 to 32 weeks of gestation in the germinal matrix (89). This data is consistent with our results since we detected that the number of blood vessels

reached its peak at 145 GA (term gestation) in the white matter regions and at 115 GA (~ 31 weeks in humans) in the subventricular zone compared to the other gestational ages studied. The increase in blood vessel number we saw at 115 GA in the subventricular zone might be a result of high metabolic demand followed by angiogenetic response to ensure adequate vascular supply. Reason for this is that the subventricular zone volume is known to reach its maximum between 25-28 weeks of gestation (95).

Vascular remodeling involves a highly coordinated break-down and build-up of the vascular basement membrane and endothelial tight junction proteins and this is mediated by matrix metalloproteinases (MMPs) (96). MMP9 is the most widely studied MMP under hypoxic-ischemic conditions both in human disease and in animal studies. We showed a significant difference between the gestational ages, regardless of growth restriction, in the percentage of MMP9-positive blood vessels in the subcortical white matter. This percentage appeared increased at 115 GA, compared to the other gestational ages in this region. We could also observe a trend of increased vascular proliferation in both FGR and control animals at 115 and 125 GA in the white matter regions, compared to 145 GA in these regions.

When it comes to the differences between the FGR group and the control group, the only significant difference we saw was increased percentage of MMP9-positive blood vessels in control animals compared to FGR animals at 115 GA in the subventricular zone. No other significant differences between the FGR group and the control group appeared in any of the parameters, gestational ages or regions. Acute hypoxia has been shown to cause a shift of blood vessel size from smaller to larger blood vessels in the cerebral white matter of fetal sheep (75). The research group at Monash University has previously also studied how chronic hypoxia affects vascular morphology in FGR sheep in the same brain regions as in this study. They found that at full-term gestation, blood vessel density and area were significantly decreased in FGR individuals, compared to controls, in the corresponding brain regions (48). This is an interesting result since in the current study we did not, in

contrast, find any differences in blood vessel morphology between FGR individuals and control individuals. However, it should be noted that quantification of blood vessels in the present study was performed at x50 magnification compared to x200 magnification in the above mentioned study, which could be a source of variation in the results. In order to improve this study, we could image the sections stained with laminin again, this time using a higher magnification. This could help us increase accuracy in our results.

If we wanted to expand this study or alter our focus, there are several ways. We could examine other regions in the brain or spinal cord, for example stain the grey matter in the cerebral cortex or hippocampus. Since the first intracerebral blood vessels in human telencephalon develop at 7 weeks of gestation (57), it might be interesting to study fetuses at even earlier gestational ages. The neuropathological outcome of FGR in fetal sheep varies depending on when the placental insufficiency is induced (43), so we could explore which differences late-onset and early-onset FGR causes in terms of cerebrovascular development.

8.1 Limitations and strengths

The major strength in this study was that we had a lot of tissue material for each staining, which produced sufficient data. For every animal, we took 9 or 12 images per section, and two sections were imaged for each animal. The averages that we ended up with for each animal were therefore accurate for that particular animal. In terms of the number of animals used in this study, the overall animal number was seven (N=7). We made sample size calculation using degree of freedom (97). According to this simple approach, our sample size was larger than necessary to prove statistically significant differences if such existed, so we had enough animals.

A potential weakness in our study is that we used three different animal cohorts that were produced several years apart from each other. Even though the surgery technique is well established, we cannot be sure that the animals were maintained identically. What also was challenging is that blood vessels have three-dimensional (3D) structure, which makes them demanding to study. We used thin coronal paraffin sections of the brain tissue, which prevents a full 3D analysis in a larger tissue volume. The results depend to a large extent on the direction of the blood vessels in each section, which in turn depends on the plane in which each section is cut. This may have caused some inaccuracies in our morphological calculations.

With respect to the laboratory work, some of our stainings did not work as expected which resulted in fewer results than originally planned. Regarding the VEGF IHC, we found out that the secondary antibody was non-specific to use in sheep tissue. Since we lack data regarding VEGF, we have limited information about angiogenesis in the animals studied in this project. With regard to double fluorescence staining for endoglin and Ki67, it most likely failed because the secondary antibody was too old and had deteriorated due to it being exposed to light and temperature changes. We chose to stain with single-label, indirect Ki67 immunohistochemistry instead of double label. Single-label technique gives us no information about which cells are proliferating, so we do not know if it is endothelial cells, pericytes or other perivascular cells. We could amend this study by performing the protocol for double label fluorescence again, using a fresh secondary antibody, in order to measure blood vessels with specifically endothelial cell proliferation. Apart from the issues with protocols that did not work, we also lost some successfully stained sections because of tissue damage or when the staining was too faint or low quality to be imaged or quantified.

When it comes to imaging of the laminin staining, the images used in this study were lower magnification than in a previous study in which our group stained with the same protocol (48), x50 instead of previously used x200. This depended on that the slides were scanned in this project, and we took the pictures with an image viewing software instead of a physical microscope. As a result,

we made a misjudgement about which magnification would be appropriate. When lower magnification images were quantified, the software most likely picked up more background staining as blood vessels and missed some real blood vessels, compared to higher magnification. The overall intensity of staining may also have affected the quantification, and the software does not distinguish capillaries, veins and arteries from each other. The luminal and the endothelial area of the blood vessels could neither be measured with this approach.

In addition, when taking the images, it was challenging to find the right regions because I lacked experience of microscopy work. We tried to image the same spot consistently in each section, but sometimes the tissue in that particular spot was damaged and the image had to be taken nearby. In addition, I was not aware of that the entire field of view was supposed to be occupied by tissue. Therefore, especially in the subventricular zone, the vessel number might be underestimated because some of the view was empty. Furthermore, the entire section was never imaged, only limited parts of it.

Regarding the statistical analysis, almost all of our data sets passed the Shapiro-Wilk normality test. However, there were 3 sets of data that were not normally distributed: blood vessel area in the subventricular zone, blood vessel length in the subcortical white matter, and percentage of MMP9-positive blood vessels in the subcortical white matter. This may have caused that we made more assumptions about the results than statistically appropriate.

9. Conclusions and implications

Our goal in this ontogeny study was to gain new knowledge about vascular maturation in the developing, growth-restricted brain during late gestation. In this way, we could contribute to the development of potential neuroprotective strategies to this vulnerable patient group in which IVH-

GMH is a major concern. The current results obtained in this study suggest that fetal growth restriction does not disrupt cerebral vascular maturation in the fetal sheep brain. Nonetheless, we obtained some interesting results that are more likely related to normal, physiological vascular development and may therefore provide new insight in the context of cerebral vascular maturation in preterm infants. During development of the central nervous system, several cell types including pericytes, smooth muscle cells and astrocytes associate with blood vessels and contribute to maturation of the brain vasculature (97). This makes vascular development a complex topic to examine. The morphological changes in the cerebral vasculature we observed at 125 GA potentially indicate a vulnerable developmental window in the brain regions we studied. These changes would need to be related to developmental changes and the whole neurovascular unit and the other angiogenetic growth factors should be investigated at this gestational age in FGR and control animals. By doing this, we could potentially identify if FGR affects the vulnerability of these particular brain regions to injury.

10. Blodkärlsutveckling i hjärnan hos fårfoster utsatta för tillväxthämning i livmodern - populärvetenskaplig sammanfattning

Brist på syre och näring under fostertiden leder till tillväxthämning, och fostret föds med lägre födelsevikt. Oftast orsakas tillväxthämningen av att moderkakan inte fungerar optimalt eftersom det är därifrån fostret får syre och näring via blodkärl. Det ger konsekvenser i många olika organ i kroppen. Det kan bland annat leda till att hjärnan inte utvecklas normalt och att barnet får sämre rörelseförmåga, inlärningsförmåga och presterar sämre i skolan. I den här studien har vi undersökt hur långvarig brist på syre och näring under graviditet påverkar utvecklingen av blodkärl i hjärnan hos fostret. Studien har genomförts på en medicinsk forskningsinstitution i Melbourne, Australien.

10.1 Metod

Vi använde oss av en väletablerad och beprövad modell av fårfoster. Ett kirurgiskt ingrepp utfördes när ca 70 % av graviditeten hade passerat. Ingreppet orsakade försämrad funktion av moderkakan som ledde till att fostret eller fostren utsattes för brist på syre och näring i livmodern. En tillväxthämmad grupp av foster avlivades sedan när ca 80 % av graviditeten hade passerat, en annan grupp när ca 85 % hade passerat, och en tredje grupp avlivades efter fullgången graviditet. Varje tillväxthämmad grupp jämfördes med en kontrollgrupp, som bestod av foster med normalfungerande moderkakor och som genomgått lika långa graviditeter som fostren i den tillväxthämmade gruppen.

Efter avlivningen opererades hjärnorna ut ur fostren och snittades i tunna snitt. Tre olika regioner i hjärnan studerades. Snitten färgades med en laboratorieteknik för att kunna visualisera kärl samt två proteiner relaterade till kärlutvecklingen. Färgningarna undersöktes med ett mikroskop och beräkningar gjordes såväl manuellt som med hjälp av ett datorprogram.

10.2 Resultat

Vi såg mycket sparsamma skillnader mellan den tillväxthämmade gruppen och kontrollgruppen. När vi jämförde graviditetslängder, såg vi att efter 80% av en fullgången graviditet fanns det ökning i ett kärltillväxtfrämjande protein i en av hjärnregionerna i fosterhjärnorna. Efter 85 % av en fullgången graviditet var kärlen generellt sett bredare, längre och hade större yta och omkrets. Vid fullgången graviditet var antalet kärl ökat i två av hjärnregionerna, jämfört med tidigare under graviditeten. Dessa fynd var likadana hos såväl de tillväxthämmade fostren som fostren med normal graviditet.

10.3 Studiens användbarhet

Hjärnan hos ett tillväxthämmat foster är sårbar och utvecklas inte normalt när den inte har fullgod tillgång till syre och näring. Dessa barn föds ofta också för tidigt vilket komplicerar situationen ytterligare. Konsekvenserna kan bli långvariga vad gäller bland annat beteende och rörelseförmåga. Enligt den här studien tar hjärnans blodkärl inte skada av tillväxthämning, men det finns fler aspekter att undersöka inom ämnet. Däremot har vi sett skillnader i kärlutvecklingen över tid i graviditeten. Denna kunskap kan hjälpa forskningen i utvecklingen av potentiella behandlingar för att förebygga och åtgärda hjärnskador hos tillväxthämmade och för tidigt födda bebisar.

11. Acknowledgements

I would like to thank my supervisors Prof Carina Mallard, A/Prof Suzie Miller and Dr Margie Castillo-Melendez for your great advice and patience. I would also like to show my gratitude to the Miller-Jenkins laboratory group at the Ritchie Center at Hudson Institute of Medical Research for welcoming me into their group and to Dr Kirstin Elglass for her technical assistance. Thank you, Stena Foundation and the Sahlgrenska Academy, for the scholarships that helped me finance my trip and stay in Melbourne.

12. Appendix

Detailed protocols for the five immunohistochemical stainings performed in this study are described below.

12.1 Laminin single-label, indirect immunohistochemistry

1. Bake the slides in 56 °C oven for one hour.

2. The following day, dewax the slides 2x5 minutes (min) in xylene and rehydrate in 2x5 minutes in 100 % ethanol and 5 minutes in 70 % ethanol. Rehydrate further for 10 minutes in phosphate-buffered saline (PBS) containing 0.1 % tween 20 (pH 7.4).

3. Apply PAP (peroxidase-anti-peroxidase) pen around tissue sections.

4. Cover the sections with 20 µg/ml Proteinase K (200 µl in TE Buffer, pH 8.0 containing NO detergent) and incubate for 30 minutes at 37 °C humidified chamber.

5. Allow sections to cool at room temperature for 20 minutes and rinse in PBS for 3x5 minutes.

6. Block endogenous peroxidases with 0.3 % hydrogen peroxide in 50 % methanol for 15 minutes at room temperature.

7. Rinse the sections were rinsed in PBS 3x5 minutes and block with DAKO protein free blocking solution for 45 minutes at room temperature to block non-specific binding.

8. Blot excess serum blocker was blotted from sections and incubate sections with rabbit anti-laminin IgG (1:200 dilution) made up in PBS overnight at 4 °C in a humidified box.

9. On the following day, rinse the sections in PBS for 3x5 minutes, incubated with a goat anti-rabbit biotinylated secondary antibody (1:200) for 1 hour at room temperature.

10. Rinse the sections in PBS for 3x5 minutes and subsequently incubate with streptavidin-horseradish peroxidase (streptavidin-HRP) 1:200 reagent for 45 minutes at room temperature and rinsed in PBS 3x5 minutes.

11. Incubate the sections with 3,3’ diaminobenzidine (DAB) complex (1/10) for 15 minutes at room temperature to allow visualisation of the immunostaining. Mix one tablet with 10ml water, vortex until the tablet was dissolved and add 3µl of hydrogen peroxide before applying 200µl to each section.

12. Wash the sections were then washed in running tap water for 2 minutes. Rehydrate through a series of ethanol baths (70% ethanol for 2 minutes, 2x100% ethanol for 2 minutes each) and clear in xylene 2x5 minutes. Coverslip with DPX mounting medium.

12.2 Double label fluorescence: endoglin and Ki67 immunohistochemistry

1. Bake the sections in 56 °C oven for one hour and dewax in xylene 2x5 minutes

2. Wash the sections in 100 % ethanol for 2x 5 minutes and in 70 % ethanol for 5 minutes. Rehydrate for 5 minutes in phosphate-buffered saline (PBS) containing 0.3% Triton X 100 (PBS-TX) (pH 7.4).

3. Antigen retrieval part 1: heat tissue sections in a microwave oven in citrate buffer at pH 6.0 for 10 minutes at 100 °. Cool for 10 minutes in hot buffer and rinsed in 3x5 minutes in PBS.

4. Block endogenous peroxidase with 3 % H_2O_2 in methanol for 5 minutes at room temperature.

5. Rinse the sections in PBS for 3 x 5 minutes.

6. Incubate with sodium borohydride (10mg/ml) in 0.01 M PBS 2x10 minutes and wash in PBS 3x5 minutes to minimize autofluorescence.

7. Incubate the sections in DAKO protein free blocker for 40 minutes at room temperature.

8. Incubate with a mixture of mouse monoclonal anti-endoglin primary antibody (1/50 millipore) and rabbit monoclonal anti-Ki-67 antibody (1:100) made up in 0.1 M PBS overnight at 4 °.

9. On the following day, wash the sections 3x5 minutes in PBS.

10. Incubate protected from light with a mix of fluorescence labelled secondary antibody, goat anti-mouse Alexa 594 (1/1000), and goat anti-rabbit Alexa A488 (1/1000).

11. Wash the sections in PBS 3x5 minutes and allow to dry.

12. Coverslip with Vectashield aqueous mounting media and store protected from light in the fridge.

12.3 VEGF single-label, indirect immunohistochemistry

1. Rinse the sections were rinsed in PBS-TX (triton X 1%) for 10 minutes.

2. Antigen retrieval was performed by heating the sections 3x10 minutes bursts in the microwave in citric acid buffer at pH 6 and cooled for 20 minutes at room temperature.

3. Rinse the sections in PBS for 3 x15 minutes.

4. Peroxidase blocking: incubate sections in peroxidase blocking solution for 10 minutes at room temperature. Reduce unspecific background staining by rinsing the sections in 0.3 % H_2O_2.

6. Rinse the sections in PBS for 3x5 minutes. Serum blocking was performed by incubating sections in DAKO protein free blocker for 60 minutes at room temperature.

7. Incubate the sections in mouse-monoclonal anti-VEGF-A primary antibody (1/200) in PBS overnight at 4 °C.

8. The following day, rinse the sections in PBS 3x5 minutes.

9. Incubate the sections in the secondary antibody goat-anti-mouse (1/200) in PBS for one hour at room temperature.

10. Rinse the sections in PBS for 3x5 minutes and incubate with streptavidin-HRP (1/200) for one hour at room temperature.

11. Rinse the sections in PBS for 3x5 minutes and incubate with DAB complex (1/10) for 5-10 minutes. Mix one tablet with 10ml water, vortex until the tablet is dissolved and add 3µl of hydrogen peroxide before applying 200µl to each section.

12. Rinse the sections in PBS 3x5 minutes and rinse in running tap water for 2-5 minutes.

13. Rehydrate the sections through a series of 95% ethanol for 1 minute, 100 % ethanol for 2x3 minutes and clear in xylene for 2 x 5 minutes. Coverslip the sections with DPX mounting medium.

12.4 MMP9 indirect, single-label immunohistochemistry

1. Bake the sections in 60 °C oven for one hour.

2. The following day, wash the sections 2x in 100 % ethanol for 5 minutes and in 70 % ethanol for 5 minutes.

3. Rehydrate the sections for 10 minutes in PBS containing 0.1 % Tween 20 (pH 7.4). Apply Pap pen around tissue sections.

4. Cover the sections with 20 µg/ml Proteinase K and incubate for 30 minutes at 37 °C humidified chamber.

5. Allow the sections to cool at room temperature for 20 minutes and rinse in PBS for 3x5 minutes.
6. Block endogenous peroxidases with 0.3 % hydrogen peroxide in 50 % methanol for 10 minutes at room temperature.

7. Rinse the sections in PBS 3x5 minutes and block with DAKO protein free blocking solution for 45 minutes at room temperature.

8. Blot excess serum blocker from sections and incubate the sections with rabbit polyclonal MMP9 (1:100 dilution) made up in PBS overnight at 4 °C in a humidified box.

9. On the following day, rinse the sections in PBS 3x5 minutes and incubate with biotinylated goat anti-rabbit IgG (1:200 dilution) for 55 minutes at room temperature.

10. Rinse the sections in PBS 3x5 minutes and incubate with streptavidin-HRP (1/200) reagent for 45 minutes at room temperature.

11. Rinse the sections in PBS 3-5 minutes and incubate with DAB complex (1/10) for 15 minutes at room temperature. Mix one tablet with 10ml water, vortex until the tablet was dissolved and add 3µl of hydrogen peroxide before applying 200µl to each section.

12. Rinse the sections in PBS 3 x 5 min and faintly counterstain by dipping the sections in 0.1% Cresyl Violet.

13. Rinse the sections quickly in tap water to remove excess stain and wash in 70% ethanol for 5 min. This is performed in order to allow identification of blood vessels without drowning out the brown DAB chromagen used to visualize MMP9 immunoreactivity.

14. Wash the sections in running tap water for 1 minute or more and dehydrate by bathing sections in 70 % EtOH for 2 minutes, and 2x100 % EtOH for 2 minutes each. Clear the sections in xylene 2x5 minutes each and coverslip with DPX mounting medium.

12.5 Ki67 single-label, indirect immunohistochemistry

1. Dewax the sections 3 x 5 min in xylene and rehydrate in 0.05M Tris-buffered saline containing 0.3 % triton x100 (PBS-TX) (pH 7.6).
2. Antigen retrieval: heat the slides in citric acid buffer (pH 6) for 4x5 min followed by 10 min cooling in the buffer.
3. Wash the sections 3 x 5 in PBS-TX at room temperature.
4. Quench endogenous peroxidases by placing slides in mailers and using 3% hydrogen peroxide in water for 10 min at room temperature. Wash the sections in PBS 3 x 5min. Draw PAP pen around each section.
5. Transfer the sections to an incubation box and incubate in DAKO protein free blocker 45 min at room temperature (200µl per section).
6. Incubate the sections with rabbit monoclonal antibody against Ki67 in PBS at room temperature 1/100 at 4ºC overnight (200µl per section).
7. The following day, rinse the sections in PBS 3 x 5 min.
8. Incubate the sections with biotinylated goat anti-rabbit secondary antibody (1/200) for 1 hour at room temperature (200µl per section).
9. Rinse the sections in PBS 3 x 5 min and incubate with strep-HRP (1/200) for 1 hour at room temperature (200µl per section).
10. Rinse the sections in PBS 3 x 5 min and incubate with DAB complex (1/10) for 5-15 min. Mix one tablet with 10ml of water, vortex until the tablet is dissolved and add 3µl of hydrogen peroxide before applying 200 µl to each section.
11. Rinse the sections in PBS 3 x 5 min and faintly counterstain by dipping the sections in 0.1% Cresyl Violet. This is performed in order to allow identification of blood vessels without drowning out the brown DAB chromagen used to visualize Ki67 immunopositive cells.

12. Rinse the sections quickly in tap water to remove excess stain and wash in 70% ethanol for 5 min. Dehydrate the sections through 2x3min changes of absolute ethanol and clear in xylene 2x3 min. Coverslip with DPX mounting medium.

12. References

1. Bamfo JEAK, Odibo AO. Diagnosis and Management of Fetal Growth Restriction. Journal of Pregnancy. 2011;2011:15.
2. Miller SL, Huppi PS, Mallard C. The consequences of fetal growth restriction on brain structure and neurodevelopmental outcome. The Journal of physiology. 2016;594(4):807-23.
3. Figueras F, Gratacos E. Update on the diagnosis and classification of fetal growth restriction and proposal of a stage-based management protocol. Fetal diagnosis and therapy. 2014;36(2):86-98.
4. Figueras F, Gardosi J. Intrauterine growth restriction: New concepts in antenatal surveillance, diagnosis, and management. American Journal of Obstetrics and Gynecology. 2011;204(4):288-300.
5. Gutaj P, Wender-Ozegowska E. Diagnosis and Management of IUGR in Pregnancy Complicated by Type 1 Diabetes Mellitus. Current Diabetes Reports. 2016;16:39.
6. Gagnon R. Placental insufficiency and its consequences. European Journal of Obstetrics & Gynecology and Reproductive Biology. 2003;110:S99-S107.
7. Lackman F, Capewell V, Gagnon R, Richardson B. Fetal umbilical cord oxygen values and birth to placental weight ratio in relation to size at birth. American Journal of Obstetrics and Gynecology. 2001;185(3):674-82.
8. Baschat Ahmet A. Fetal growth restriction – from observation to intervention. Journal of Perinatal Medicine2010. p. 239.
9. McMillen IC, Adams MB, Ross JT, Coulter CL, Simonetta G, Owens JA, et al. Fetal growth restriction: Adaptations and consequences. Reproduction. 2001;122(2):195-204.
10. Yanney M, Marlow N. Paediatric consequences of fetal growth restriction. Seminars in Fetal and Neonatal Medicine. 2004;9(5):411-8.
11. Guellec I, Lapillonne A, Renolleau S, Charlaluk M-L, Roze J-C, Marret S, et al. Neurologic Outcomes at School Age in Very Preterm Infants Born With Severe or Mild Growth Restriction. Pediatrics. 2011;127(4):e883.
12. Morsing E, Åsard M, Ley D, Stjernqvist K, Maršál K. Cognitive function after intrauterine growth restriction and very preterm birth. Pediatrics. 2011;127(4):e874-e82.
13. TrØNnes H, Wilcox AJ, Lie RT, Markestad T, Moster DAG. Risk of cerebral palsy in relation to pregnancy disorders and preterm birth: a national cohort study. Developmental medicine and child neurology. 2014;56(8):779-85.
14. Arduini D, Rizzo G, Caforio L, Boccolini MR, Romanini C, Mancuso S. Behavioural state transitions in healthy and growth retarded fetuses. Early Human Development. 1989;19(3):155-65.
15. Harvey D, Prince J, Bunton J, Parkinson C, Campbell S. Abilities of children who were small-for-gestational-age babies. Pediatrics. 1982;69(3):296-300.
16. Kaukola T, Räsänen J, Herva R, Patel DD, Hallman M. Suboptimal neurodevelopment in very preterm infants is related to fetal cardiovascular compromise in placental insufficiency. American Journal of Obstetrics and Gynecology. 2005;193(2):414-20.
17. Baschat AA. Neurodevelopment after fetal growth restriction. Fetal diagnosis and therapy. 2014;36(2):136-42.
18. Tolsa CB, Zimine S, Warfield SK, Freschi M, Sancho Rossignol A, Lazeyras F, et al. Early alteration of structural and functional brain development in premature infants born with intrauterine growth restriction. Pediatric research. 2004;56(1):132-8.
19. Samuelsen GB, Pakkenberg B, Bogdanović N, Gundersen HJG, Larsen JF, Græm N, et al. Severe cell reduction in the future brain cortex in human growth–restricted fetuses and infants. American Journal of Obstetrics and Gynecology. 2007;197(1):56.e1-.e7.
20. Dubois J, Benders M, Borradori-Tolsa C, Cachia A, Lazeyras F, Ha-Vinh Leuchter R, et al. Primary cortical folding in the human newborn: an early marker of later functional development. Brain. 2008;131(8):2028-41.
21. Anand KS, Dhikav V. Hippocampus in health and disease: An overview. Annals of Indian Academy of Neurology. 2012;15(4):239-46.
22. Sizonenko SV, Borradori-Tolsa C, Vauthay DM, Lodygensky G, Lazeyras F, Hüppi PS. Impact of intrauterine growth restriction and glucocorticoids on brain development: Insights using advanced magnetic resonance imaging. Molecular and Cellular Endocrinology. 2006;254-255:163-71.
23. Lodygensky GA, Seghier ML, Warfield SK, Tolsa CB, Sizonenko S, Lazeyras F, et al. Intrauterine growth restriction affects the preterm infant's hippocampus. Pediatric research. 2008;63(4):438-43.
24. Eixarch E, Muñoz-Moreno E, Bargallo N, Batalle D, Gratacos E. Motor and cortico-striatal-thalamic connectivity alterations in intrauterine growth restriction. American Journal of Obstetrics and Gynecology. 2016;214(6):725.e1-.e9.

25. Fischi-Gómez E, Vasung L, Meskaldji D-E, Lazeyras F, Borradori-Tolsa C, Hagmann P, et al. Structural Brain Connectivity in School-Age Preterm Infants Provides Evidence for Impaired Networks Relevant for Higher Order Cognitive Skills and Social Cognition. Cerebral Cortex. 2015;25(9):2793-805.
26. Saunavaara V, Kallankari H, Parkkola R, Haataja L, Olsén P, Hallman M, et al. Very preterm children with fetal growth restriction demonstrated altered white matter maturation at nine years of age. Acta Paediatrica, International Journal of Paediatrics. 2017;106(10):1600-7.
27. Tolcos M, Petratos S, Hirst JJ, Wong F, Spencer SJ, Azhan A, et al. Blocked, delayed, or obstructed: What causes poor white matter development in intrauterine growth restricted infants? Progress in Neurobiology. 2017;154:62-77.
28. Takashima S, Tanaka K. Development of cerebrovascular architecture and its relationship to periventricular leukomalacia. Archives of Neurology. 1978;35(1):11-6.
29. Ortigosa Rocha C, Bittar RE, Zugaib M. Neonatal Outcomes of Late-Preterm Birth Associated or Not with Intrauterine Growth Restriction. Obstetrics and Gynecology International. 2010;2010.
30. Back SA, Luo NL, Borenstein NS, Levine JM, Volpe JJ, Kinney HC. Late oligodendrocyte progenitors coincide with the developmental window of vulnerability for human perinatal white matter injury. Journal of Neuroscience. 2001;21(4):1302-12.
31. Basilious A, Yager J, Fehlings MG. Neurological outcomes of animal models of uterine artery ligation and relevance to human intrauterine growth restriction: a systematic review. Developmental Medicine & Child Neurology. 2015;57(5):420-30.
32. Tashima L, Nakata M, Anno K, Sugino N, Kato H. Prenatal influence of ischemia-hypoxia-induced intrauterine growth retardation on brain development and behavioral activity in rats. Biology of the neonate. 2001;80(1):81-7.
33. Delcour M, Russier M, Amin M, Baud O, Paban V, Barbe MF, et al. Impact of prenatal ischemia on behavior, cognitive abilities and neuroanatomy in adult rats with white matter damage. Behavioural Brain Research. 2012;232(1):233-44.
34. Tolcos M, Bateman E, O'Dowd R, Markwick R, Vrijsen K, Rehn A, et al. Intrauterine growth restriction affects the maturation of myelin. Experimental Neurology. 2011;232(1):53-65.
35. Olivier P, Baud O, Bouslama M, Evrard P, Gressens P, Verney C. Moderate growth restriction: Deleterious and protective effects on white matter damage. Neurobiology of Disease. 2007;26(1):253-63.
36. Miller SL, Yawno T, Alers NO, Castillo-Melendez M, Supramaniam VG, Vanzyl N, et al. Antenatal antioxidant treatment with melatonin to decrease newborn neurodevelopmental deficits and brain injury caused by fetal growth restriction. Journal of Pineal Research. 2014;56(3):286-94.
37. Delcour M, Olivier P, Chambon C, Pansiot J, Russier M, Liberge M, et al. Neuroanatomical, Sensorimotor and Cognitive Deficits in Adult Rats with White Matter Injury Following Prenatal Ischemia. Brain Pathology. 2012;22(1):1-16.
38. Loya CM, Van Vactor D, Fulga TA. Understanding neuronal connectivity through the post-transcriptional toolkit. Genes & Development. 2010;24(7):625-35.
39. Eixarch E, Batalle D, Illa M, Muñoz-Moreno E, Arbat-Plana A, Amat-Roldan I, et al. Neonatal Neurobehavior and Diffusion MRI Changes in Brain Reorganization Due to Intrauterine Growth Restriction in a Rabbit Model. PLOS ONE. 2012;7(2):e31497.
40. Fung C, Ke X, Brown AS, Yu X, McKnight RA, Lane RH. Uteroplacental insufficiency alters rat hippocampal cellular phenotype in conjunction with ErbB receptor expression. Pediatric research. 2012;72(1):2-9.
41. Mallard C, Loeliger M, Copolov D, Rees S. Reduced number of neurons in the hippocampus and the cerebellum in the postnatal guinea-pig following intrauterine growth-restriction. Neuroscience. 2000;100(2):327-33.
42. Illa M, Eixarch E, Batalle D, Arbat-Plana A, Muñoz-Moreno E, Figueras F, et al. Long-Term Functional Outcomes and Correlation with Regional Brain Connectivity by MRI Diffusion Tractography Metrics in a Near-Term Rabbit Model of Intrauterine Growth Restriction. PLoS ONE. 2013;8(10).
43. Alves de Alencar Rocha AK, Allison BJ, Yawno T, Polglase GR, Sutherland AE, Malhotra A, et al. Early- versus Late-Onset Fetal Growth Restriction Differentially Affects the Development of the Fetal Sheep Brain. Developmental neuroscience. 2017;39(1-4):141-55.
44. Hawkins BT, Davis TP. The blood-brain barrier/neurovascular unit in health and disease. Pharmacological Reviews. 2005;57(2):173-85.
45. Obermeier B, Daneman R, Ransohoff RM. Development, maintenance and disruption of the blood-brain barrier. Nature medicine. 2013;19(12):1584-96.
46. Abbott NJ, Rönnbäck L, Hansson E. Astrocyte-endothelial interactions at the blood-brain barrier. Nature Reviews Neuroscience. 2006;7(1):41-53.
47. Ransohoff RM, Engelhardt B. The anatomical and cellular basis of immune surveillance in the central nervous system. Nature Reviews Immunology. 2012;12:623.

48. Castillo-Melendez M, Yawno T, Allison BJ, Jenkin G, Wallace EM, Miller SL. Cerebrovascular adaptations to chronic hypoxia in the growth restricted lamb. International journal of developmental neuroscience : the official journal of the International Society for Developmental Neuroscience. 2015;45:55-65.
49. Winkler EA, Bell RD, Zlokovic BV. Central nervous system pericytes in health and disease. Nature Neuroscience. 2011;14:1398.
50. Gee JR, Keller JN. Astrocytes: regulation of brain homeostasis via apolipoprotein E. The International Journal of Biochemistry & Cell Biology. 2005;37(6):1145-50.
51. Carvey PM, Hendey B, Monahan AJ. The blood–brain barrier in neurodegenerative disease: a rhetorical perspective. Journal of Neurochemistry. 2009;111(2):291-314.
52. Persidsky Y, Ramirez SH, Haorah J, Kanmogne GD. Blood-brain barrier: Structural components and function under physiologic and pathologic conditions. Journal of Neuroimmune Pharmacology. 2006;1(3):223-36.
53. Rascher G, Fischmann A, Kröger S, Duffner F, Grote E-H, Wolburg H. Extracellular matrix and the blood-brain barrier in glioblastoma multiforme: spatial segregation of tenascin and agrin. Acta Neuropathologica. 2002;104(1):85-91.
54. Scholler K, Trinkl A, Klopotowski M, Thal SC, Plesnila N, Trabold R, et al. Characterization of microvascular basal lamina damage and blood-brain barrier dysfunction following subarachnoid hemorrhage in rats. Brain Res. 2007;1142:237-46.
55. Baburamani AA, Ek CJ, Walker DW, Castillo-Melendez M. Vulnerability of the developing brain to hypoxic-ischemic damage: Contribution of the cerebral vasculature to injury and repair? Frontiers in Physiology. 2012;3 NOV.
56. Tomanek RJ, Schatteman GC. Angiogenesis: New insights and therapeutic potential. Anatomical Record. 2000;261(3):126-35.
57. Korzhevskii DE, Otellin VA. Initial stage of vascular bed development in telencephalon of human embryo. Bulletin of experimental biology and medicine. 2000;129(5):508-10.
58. Rakocevic J, Orlic D, Mitrovic-Ajtic O, Tomasevic M, Dobric M, Zlatic N, et al. Endothelial cell markers from clinician's perspective. Experimental and Molecular Pathology. 2017;102(2):303-13.
59. Timpl R, Rohde H, Robey PG, Rennard SI, Foidart JM, Martin GR. Laminin - A glycoprotein from basement membranes. Journal of Biological Chemistry. 1979;254(19):9933-7.
60. Risau W, Lemmon V. Changes in the vascular extracellular matrix during embryonic vasculogenesis and angiogenesis. Developmental Biology. 1988;125(2):441-50.
61. Yurchenco PD, Schittny JC. Molecular architecture of basement membranes. FASEB Journal. 1990;4(6):1577-90.
62. Liesi P. Do neurons in the vertebrate CNS migrate on laminin? The EMBO Journal. 1985;4(5):1163-70.
63. Liesi P, Kaakkola S, Dahl D, Vaheri A. Laminin is induced in astrocytes of adult brain by injury. EMBO Journal. 1984;3(3):683-6.
64. Milner R, Campbell IL. Developmental Regulation of β1 Integrins during Angiogenesis in the Central Nervous System. Molecular and Cellular Neuroscience. 2002;20(4):616-26.
65. Scholzen T, Gerdes J. The Ki-67 protein: from the known and the unknown. Journal of cellular physiology. 2000;182(3):311-22.
66. Hitchman E, Hodgkinson C, Roberts D, Ashton G, Yunus Z, Byers R, et al. Effect of prolonged formalin fixation on immunohistochemical staining for the proliferation marker Ki67. Histopathology. 2011;59(6):1261-3.
67. Yang Y, Kimura-Ohba S, Thompson JF, Salayandia VM, Cossé M, Raz L, et al. Vascular tight junction disruption and angiogenesis in spontaneously hypertensive rat with neuroinflammatory white matter injury. Neurobiology of Disease. 2018;114:95-110.
68. Keck PJ, Hauser SD, Krivi G, Sanzo K, Warren T, Feder J, et al. Vascular permeability factor, an endothelial cell mitogen related to PDGF. Science (New York, NY). 1989;246(4935):1309-12.
69. Carmeliet P. Angiogenesis in health and disease. Nature medicine. 2003;9:653.
70. Sondell M, Lundborg G, Kanje M. Vascular Endothelial Growth Factor Has Neurotrophic Activity and Stimulates Axonal Outgrowth, Enhancing Cell Survival and Schwann Cell Proliferation in the Peripheral Nervous System. The Journal of Neuroscience. 1999;19(14):5731.
71. Dirk Matthias H, Anil Z. Implications of Vascular Endothelial Growth Factor for Postischemic Neurovascular Remodeling. Journal of Cerebral Blood Flow & Metabolism. 2009;29(10):1620-43.
72. Breier G, Albrecht U, Sterrer S, Risau W. Expression of vascular endothelial growth factor during embryonic angiogenesis and endothelial cell differentiation. Development. 1992;114(2):521.
73. del Zoppo GJ, Mabuchi T. Cerebral microvessel responses to focal ischemia. Journal of cerebral blood flow and metabolism : official journal of the International Society of Cerebral Blood Flow and Metabolism. 2003;23(8):879-94.
74. Krupinski J, Kaluza J, Kumar P, Kumar S, Wang JM. Role of angiogenesis in patients with cerebral ischemic stroke. Stroke. 1994;25(9):1794-8.

75. Baburamani AA, Lo C, Castillo-Melendez M, Walker DW. Morphological evaluation of the cerebral blood vessels in the late gestation fetal sheep following hypoxia in utero. Microvascular research. 2013;85:1-9.
76. Zhang ZG, Zhang L, Jiang Q, Chopp M. Bone Marrow-Derived Endothelial Progenitor Cells Participate in Cerebral Neovascularization After Focal Cerebral Ischemia in the Adult Mouse. Circulation Research. 2002;90(3):284.
77. Zalewska T, Ziemka-Nalecz M, Sarnowska A, Domanska-Janik K. Involvement of MMPs in delayed neuronal death after global ischemia. Acta neurobiologiae experimentalis. 2002;62(2):53-61.
78. Rosenberg GA. Matrix metalloproteinases in neuroinflammation. Glia. 2002;39(3):279-91.
79. Minoru A, Kazuko A, Jae-Chang J, Gregory JdZ, Fini ME, Eng HL. Role for Matrix Metalloproteinase 9 after Focal Cerebral Ischemia: Effects of Gene Knockout and Enzyme Inhibition with BB-94. Journal of Cerebral Blood Flow & Metabolism. 2000;20(12):1681-9.
80. Asahi M, Wang X, Mori T, Sumii T, Jung JC, Moskowitz MA, et al. Effects of matrix metalloproteinase-9 gene knock-out on the proteolysis of blood-brain barrier and white matter components after cerebral ischemia. The Journal of neuroscience : the official journal of the Society for Neuroscience. 2001;21(19):7724-32.
81. Svedin P, Hagberg H, Savman K, Zhu C, Mallard C. Matrix metalloproteinase-9 gene knock-out protects the immature brain after cerebral hypoxia-ischemia. The Journal of neuroscience : the official journal of the Society for Neuroscience. 2007;27(7):1511-8.
82. Schoch HJ, Fischer S, Marti HH. Hypoxia-induced vascular endothelial growth factor expression causes vascular leakage in the brain. Brain. 2002;125(Pt 11):2549-57.
83. Witt KA, Mark KS, Hom S, Davis TP. Effects of hypoxia-reoxygenation on rat blood-brain barrier permeability and tight junctional protein expression. American Journal of Physiology-Heart and Circulatory Physiology. 2003;285(6):H2820-H31.
84. Gonul E, Duz B, Kahraman S, Kayali H, Kubar A, Timurkaynak E. Early pericyte response to brain hypoxia in cats: an ultrastructural study. Microvascular research. 2002;64(1):116-9.
85. Ferrari DC, Nesic OB, Perez-Polo JR. Oxygen resuscitation does not ameliorate neonatal hypoxia/ischemia-induced cerebral edema. Journal of neuroscience research. 2010;88(9):2056-65.
86. Ek CJ, D'Angelo B, Baburamani AA, Lehner C, Leverin AL, Smith PL, et al. Brain barrier properties and cerebral blood flow in neonatal mice exposed to cerebral hypoxia-ischemia. Journal of cerebral blood flow and metabolism : official journal of the International Society of Cerebral Blood Flow and Metabolism. 2015;35(5):818-27.
87. Sutherland AE, Crossley KJ, Allison BJ, Jenkin G, Wallace EM, Miller SL. The effects of intrauterine growth restriction and antenatal glucocorticoids on ovine fetal lung development. Pediatric research. 2012;71(6):689-96.
88. Back SA. White matter injury in the preterm infant: pathology and mechanisms. Acta Neuropathologica. 2017;134(3):331-49.
89. Ballabh P, Braun A, Nedergaard M. Anatomic analysis of blood vessels in germinal matrix, cerebral cortex, and white matter in developing infants. Pediatric research. 2004;56(1):117-24.
90. Pekcevik Y, Pasinli A, Arun Ozer E, Erdogan N. Risk factors of germinal matrix intraventricular hemorrhage in premature infants. Iranian Journal of Pediatrics. 2014;24(2):191-7.
91. Tsimis ME, Johnson CT, Raghunathan RS, Northington FJ, Burd I, Graham EM. Risk factors for periventricular white matter injury in very low birthweight neonates. American Journal of Obstetrics and Gynecology. 2016;214(3):380.e1-.e6.
92. Taylor CR, Shi SR, Barr NJ. Techniques of Immunohistochemistry. Principles, Pitfalls, and Standardization. Diagnostic Immunohistochemistry2010. p. 1-41.
93. McIntire DD, Leveno KJ. Neonatal mortality and morbidity rates in late preterm births compared with births at term. Obstetrics and Gynecology. 2008;111(1):35-41.
94. Mito T, Konomi H, Houdou S, Takashima S. Immunohistochemical study of the vasculature in the developing brain. Pediatric neurology. 1991;7(1):18-22.
95. Volpe JJ. The Encephalopathy of Prematurity—Brain Injury and Impaired Brain Development Inextricably Intertwined. Seminars in Pediatric Neurology. 2009;16(4):167-78.
96. Galis ZS, Khatri JJ. Matrix Metalloproteinases in Vascular Remodeling and Atherogenesis. Circulation Research. 2002;90(3):251.
97. Arnold T, Betsholtz C. The importance of microglia in the development of the vasculature in the central nervous system. Vascular Cell; Vol 5 No 1 (2013): VascularCell. 2013.